Universidade de Aveiro Departamento de Cerâmica e Vidro
2009

Fikadu Legesse
Alema

Híbridos orgânicos-inorgânicos dopados com corantes rodaminas para aplicação em dispositivos emissores de luz

Organic-inorganic hybrid doped with rhodamine dyes for light emitting applications

Universidade de Aveiro Departamento de Cerâmica e Vidro
2009

Fikadu Legesse Alema

Híbridos orgânicos-inorgânicos dopados com corantes rodaminas para aplicação em dispositivos emissores de luz

Organic-inorganic hybrid doped with rhodamine dyes for light emitting applications

Dissertação apresentada à Universidade de Aveiro para cumprimento dos requisitos necessários à obtenção do grau de Mestre do Mestrado Europeu em Ciência dos Materiais sob realizadar orientação científica do Doutor Luís António Ferreira Martins Dias Carlos, Professor catedrático no departamento de física da Universidade de Aveiro, Doutor Edison Pecoraro, Investigador Auxiliar no Instituto de Telecomunicações – Aveiro e do Doutor Lars Rosgaard Jensen Professor Associado do Departamento de Engenharia Mecânica da Aalborg Universitet.

A dissertation presented to the University of Aveiro in partial fulfilment of the requirements for the awarding of the Joint European Master degree in Materials Science carried out under the supervision of Luís António Ferreira Martins Dias Carlos, Full professor at the Physics Department of University of Aveiro, Dr. Edison Pecoraro, Assistant researcher at the Institute of telecommunication, Aveiro and Lars Rosgaard Jensen, Associate Professor at the Mechanical Engineering Department of Aalborg University.

O júri

Presidente

Prof. Doutor Vítor Brás Sequeira Amaral
Professor Associado com Agregação da Universidade de Aveiro, Portugal

Prof. Doutora Verónica Cortés de Zea Bermudez
Professora Associada com Agregação da Universidade de Trás-os-Montes e Alto Douro, Vila Real, Portugal

Prof. Doutor Luís António Ferreira Martins Dias Carlos
Professor catedrático da Universidade de Aveiro, Aveiro, Portugal

Doutor Edison Pecoraro
Investigador Auxiliar no Instituto de Telecomunicações da Universidade de Aveiro, Aveiro, Portugal

Prof. Doutor Lars Rosgaard Jensen
Professor Associado da Aalborg Universitet, Aalborg, Denmark

Acknowledgments

I would like to thank all who in one way or another helped me to get this work done.

First of all, I would like to thank my supervisors, Prof. Luis Dias Carlos, Dr. Edison Pecoraro and Dr. Lars Rosgaard Jensen for their supports during the entire work of this thesis. I'm happy for my association with them and share their research experiences.

I'm thankful to Prof. M. R. S. Ferreira for her assistance during the experimental work, critical reading and comment of the thesis. I would like to extend my appreciation to Sonia Nobre a PhD student at physics department of Aveiro University for her technical assistance during the PL measurements.

Finally, I would like to thank the European commission for the financial support it has given me to involve in the program of European Masters in Materials Science.

Palavras-chave

Híbridos orgânico-inorgânicos, rodamina 6G, rodamina B, foto-luminescência, absorção, XRD

Resumo

Materiais híbridos orgânico-inorgânicos dopados com corantes orgânicos, rodamina 6G e B (R6G e RB), foram caracterizados por espectroscopia de absorção, fotoluminescência e difracção de raios-X. As matrizes são constituídas por redes siliciosas covalentemente ligadas por pontes de ureia a nove unidades de oxietileno (CH2CH2O) e são conhecidas como material híbrido di-ureasil.

Os padrões de difracção dos pós e os espectros de fotoluminescência mostram que os corantes orgânicos se encontram fortemente associados ao domínio do material híbrido di-ureasil. Os espectros de emissão registados para amostras dopadas com corantes de baixa concentração (0.008%) apresentam duas bandas de emissão na gama de baixo e alto comprimento de onda. Estas duas bandas de emissão são provenientes do híbrido di-ureasil e dos corantes indicando que ambos são materiais opticamente activos. Quando a concentração dos corantes é aumentada de 0.008% para 0.1% são feitas duas observações. A primeira indica que a emissão proveniente do híbrido di-ureasil a baixa concentração foi suprimida. Isto exprime claramente que existe uma forte transferência de energia do híbrido di-ureasil para as moléculas de corante. Os espectros de excitação do di-ureasil e do corante também confirmam a presença de transferência de energia do híbrido para o corante.

A segunda consiste no facto de que a emissão proveniente do corante é deslocada para o vermelho e a banda é acompanhada por desdobramentos. Isto mostra a presença de mais do que um componente emissor devido a diferentes tipos de agregados de corante. Esta evidência é também confirmada por espectroscopia de absorção uma vez que o pico de absorção é deslocado para o vermelho com a concentração.

O aumento nas intensidades de emissão dos materiais é também observado com o aumento na concentração dos corantes. Isto foi manifestado também no rendimento quântico absoluto de emissão dos materiais. Os rendimentos quânticos absolutos de emissão de 65% para amostras dopadas com RB e de 70% para amostras dopadas com R6G com concentração de 0.1% indicam que os materiais híbridos têm elevado rendimento quântico de emissão, colocando-os como candidatos para aplicações de emissão de luz.

O resultado de XRD exibe um padrão idêntico ao padrão de difracção do di-ureasil não dopado indicando que o corante incorporado não altera as características estruturais dos di-ureasil não dopados. No entanto, a posição 2θ significativa da interferência de difusão interparticular do domínio silicioso num meio polimérico [28] é deslocada para um valor inferior em 1.5º. Isto sugere que os corantes orgânicos são incorporados no domínio orgânico do híbrido di-ureasil.

Key words

Organic inorganic hybrids, rhodamine B, rhodamine 6G, photoluminescence, absorption, XRD

Abstract

Organic-inorganic hybrid materials doped with organic dyes, rhodamine 6G and B (R6G and RB), were characterized with absorption spectroscopy, photoluminescence, and X-ray diffraction techniques. The host matrix is a silica-based network to which nine oxyethylene (CH2CH2O) repeat units are covalently grafted by urea linkages and is known as di-ureasil hybrid material.

The x-ray powder diffraction patterns and photoluminescence spectra show that the organic dyes are entrapped strongly in the organic domain of the di-ureasil hybrid material. The emission spectra recorded for samples doped with dyes of low concentration (0.008%) have two emission bands at low and high wavelength ranges. These two emission bands are due to the emissions both from the di-ureasil hybrid and the dyes indicating that both the host and the guest are optically active materials. When the concentration of the dyes increase from 0.008% to 0.1% there are two things observed. The first one is that the emission from the di-ureasil hybrid is suppressed from where it existed when the concentration was low. This clearly indicates that there is strong energy transfer from the di-ureasil hybrid to the dye molecules. The excitation spectra of the di-ureasil and the dye further confirmed the presence of an energy transfer from the host to the dye.

The second thing was that the emission from the dye was observed red shifted and the band was accompanied by shoulders. This shows the presence of more than one emitting components which are due to different types of dye aggregates. This is also confirmed by the absorption spectroscopy as the absorption peak is red shifted with concentration.

The increase in the emission intensities of the materials is also observed with the increase in the concentration of the dyes. This was also manifested in the absolute emission quantum yield of the material. The absolute emission quantum yields of 65% for RB and 70% for R6G doped samples with concentration of 0.1% signify that the hybrid materials have large emission quantum yield which put them as candidates for light emitting applications.

The XRD result shows a pattern similar with the diffraction pattern of neat di-ureasil hybrid material indicating that the incorporated dye does not alter the structural features of the neat di-ureasil. Nonetheless, a 2θ position signifying the interparticle scattering interference of the siliceous domain in a polymer rich medium [28] is shifted to lower value by 1.5º. This suggests that the organic dyes are incorporated in the organic domain of the di-ureasil hybrid.

Table of contents

Table of Figures

List of tables

List of abbreviations

d-UPTES- di-ureapropyltriethoxysilane

ICPTES-3-isocyanatopropyltriethoxysilane

PL- Photoluminescence

TRES-time resolved emission spectrum

UV- ultraviolet

XRD- X-ray diffraction

RT-room temperature

LT-low temperature

IC-internal conversion

ISC-intersystem crossing

RB-rhodamine B

R6G-rhodamine 6G

Chapter 1: Introduction

Over the past years the photochemical and photophysical properties of fluorescent dyes in solid matrices have attracted great interest. There are plentiful optical applications from dyes since they can be utilized as guest-host liquid crystal displays (LCDs) [1, 2], as guest dopants in organic LEDs, for energy transfer experiments, for pH sensing device and the majority is in use as dye lasers [3]. Fluorescent dyes are also essential for biological and medical applications. They are used in DNA sequencing, immunoassay, molecular beacon, hybridization assay, etc [4].

As mentioned above, the majority of the dyes are used as a laser medium. For us to have an overview of the research progress of doping organic dyes into a solid matrix for application in optical materials, let's focus on the dye lasers.

Dye lasers have been sources of coherent tunable radiation because of their unique operational flexibilities and fine-tune properties with emission from near ultraviolet to near infrared [5, 6]. While dyes have been demonstrated to lase in the solid, liquid or gas phases, liquid solution of dyes in suitable organic solvents have been the most frequently used lasers. This is because active medium can be obtained in high optical quality, the cooling can be achieved by a flow system, and the medium is self repairable to some extent [5].

Liquid dye lasers have been used in various applications where tunable high power and high pulse energy beams are required, such as nonlinear optics, medicine, and industry [6]. These lasers rely on the flow of dye through a laser cavity to avoid thermal problems, associated with reduction in beam quality and efficiency from heating of the gain medium and degradation of the dyes.

The self repairing ability of the dye medium in a liquid state is to an extent. High temperature as well as high local intensity of pumping light can have possibilities to degrade the dyes and eventually limit the life time of the laser. Because of these thermal and photodegradation, it is necessary for the dye solution to be changed periodically [7]. This solution often involves volatile solvent, which may be untidy, flammable, and can cause health hazard [8].

To overcome these problems and many more others related to environment, and cumbersome system design for continuous circulation of dyes [9] which limits the portability of this laser, considerable amount of efforts have been made and are being made to fabricate

tunable solid state dye laser in which an organic dye is incorporated into suitable solid matrices [7, 10, 11].

A number of materials, including organic and inorganic polymers have been tried as solid hosts for laser dyes. Organic polymers such as poly (methyl methacrylate) (PMMA) [7], poly (acrylic acid) (PAA) [9], polycarbonate, polyvinyl alcohol [9] have been used as hosts for laser dyes. Furthermore, silica based inorganic polymers such as alumosilicates [3], laponite clay [12], titania-silica, titania-ormosil, and silica-zirconia [3] materials have been investigated.

Polymers are attractive materials to be used as host because of their high optical homogeneity, good chemical compatibility with organic dyes, and the ease to modify their structure and chemical composition which allow introducing controlled changes to optimize their properties [13]. However, pure organic or polymeric solid state dye lasers suffer from thermal degradation under laser irradiation, which can shorten significantly their useful lifetimes [9].

On the other hand, inorganic solid matrices can provide high photoluminescent materials, which not only improve laser performances such as quantum yield and efficiency, but also increase the thermal and photostability of the dyes [12, 14]. The rigid structures of the inorganic matrices provide constrained environment to the dopant (dye) molecules and limits their internal degree of freedom. As a result of this, the internal conversion processes decrease and improve the fluorescence quantum yield, and consequently their laser efficiency [15]. Nevertheless, pure inorganic matrix also suffers from high processing temperature which may degrade the dye molecules during the synthesis. Or if the incorporation of the dyes may be done after preparing the template (host), by adsorption process or intercalation chemistry, then the problem of inhomogeneous distribution of the dye molecules affects the performances of the final products [12]. Therefore, there should be a compromise between the organic polymers and the inorganic solids to get properties from both of them in one host.

One celebrated way to improve the host materials without losing the benefits provided by organic polymer as well as inorganic solid is using both of them in one; i.e. organic-inorganic hybrid materials. In the organic-inorganic hybrid materials, the inorganic part ensures the rigidity of the network and may be dense enough to provide the necessary mechanical properties to obtain optical polishing and transparency properties [10, 14]. It may

also provide thermal resistance which is needed to achieve stable operations. The organic part on the other hand provides an environment favourable (for instance, hydrophobicity to repel residual polar solvents and protect the dye from chemical degradation) to the fluorescence emission of the encapsulated dye [10, 14]. Moreover, the sol-gel processing technique used for preparation of the organic inorganic host materials is also an elegant route which makes the incorporation or doping of organic dyes easier. In this processing route the dye does not suffer from high processing temperature as opposed to the processing of inorganic solid hosts.

In this work, the doping of two organic dyes, rhodamine B and 6G, into an organic-inorganic hybrid host material was preformed through sol-gel process. The structures of rhodamine 6G and B dyes are shown below in Figure 1 [3, 8]. The difference between these two dyes depends on the variation of substituents which are attached to the main xanthene structure. This difference in structure is responsible for the differences in the optical features of the two dyes which could be shifting, broadening, etc.

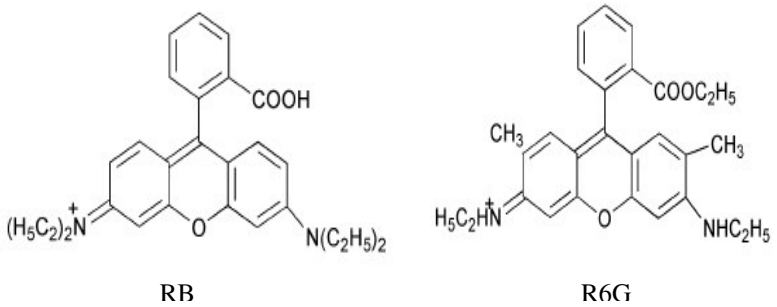

Figure 1: Structures of rhodamine B and 6G [3].

The host material employed is composed of siliceous framework to which short poly (oxyethylene) (POE) (about nine oxyethylene (CH_2CH_2O) units) chains are covalently bonded through urea (-NH(C (=O) NH) linkages. Because of the double urea bridges, this hybrid material is known as di-ureasil hybrid material. The main aim of this thesis is to characterise the as-synthesised materials with the help of photoluminescence, absorption and x-ray powder diffraction techniques to explore their optical and structural properties.

The rest of the work is presented as follows: Chapter 2 is devoted to the discussion of hybrid materials. In this chapter topics such as historical development, advantages, applications, and classification of hybrid materials are considered and discussed. Chapter 3 presents the general background of sol-gel techniques. Sol-gel is an ideal synthesis route

which is used to make the doping of organic dyes at a relatively low temperature such that the dye will not suffer from processing temperature which could lead to dye degradation. In this chapter, the general overview of sol-gel process, hydrolysis and condensation are considered and discussed. A brief introduction about amine functionalized hybrid materials was also included. In Chapter 4 the theoretical background of the characterization techniques used in this thesis are presented. The theoretical principles of absorption, photoluminescence, and x-ray diffraction processes are described. The physical processes (deactivation routes) such as: vibrational relaxation, internal conversion, intersystem crossing, fluorescence, and phosphorescence which follow after a molecule is excited to the higher energy level are discussed in detail using Jablonski diagram.

In Chapter 5 the steps taken to synthesis the material under study is presented. In addition to this description about the measurement techniques are included. The result and discussion part of the work is presented in Chapter 6. Here, the absorption, PL, and XRD results are presented and discussed. Finally, in Chapter 7 concluding remarks and some future out looks of the work are given.

Chapter 2: Hybrid materials

Hybrid materials are made by combing the often unrelated organic and inorganic materials. They come together with independent properties of their own and craft a material with completely different properties which are intended to be used for a pre-designed application [16]. The properties they may show could be the resultant of the properties between the two original phases or a different property which has no relation with either of the phases [16, 17]. The organic-inorganic hybrid material is of course beyond a simple physical combination of organic and inorganic moieties. It ranges from simple mixture to a strongly bonded compound between host and guest constituents which affects the properties of the materials depending on the scale of interaction between them. As a result, the properties of hybrid materials could range from a simple sum of the properties of the two worlds to the completely different one. The interplay between the organic and inorganic components offers the possibility of designing materials to one's very demanding specification. Besides, it makes possible to give the material with one or more specific functionalities where none existed earlier [18]. In the next few subsections we will consider the historical development, advantages, applications and classifications of the hybrid materials.

2. 1 Historical development of hybrid materials

The art of combining materials of dissimilar properties to produce improved materials is not new; it goes way back to ancient construction materials like adobe [19].
Adobe is a natural building material made from sand, clay and water, with some kind of fibrous or organic material (sticks, straw, dung), which is shaped into bricks using frames and dried in the sun. In this hybrid material the organic component (e.g. straw) is responsible for the mechanical properties of the clay. Adobe structures are extremely durable and account for some of the oldest extant buildings on the planet. Thus, it is as old as human civilization since the practice of combining the organic and inorganic moieties to create material with superior properties is started. Nevertheless, as mentioned above the concept of hybrid materials goes way beyond simple mixture of the components. Of course, the concept of hybrid falls between mixture and compound. A compound is formed by a chemical reaction between the two components, where the properties of each of them are completely changed and a new material with new property is formed. And in mixture a

physical interaction between the components is involved. Figure 2 shows a photograph of adobe material shaped in the form of bricks which are ready for building.

Figure 2: Adobe bricks ready for building [19b].

Another example of an ancient man made hybrid material is the Maya blue colour that still maintains its bright colour since 8th century (see Figure 3) [16b, 17]. Besides the beautiful blue colour paint which is harmless to the environment, it shows resistance to acid, alkaline solvents, oxidants, reductors, temperature, and bio corrosion [19c]. The reason why the Maya blue colour kept its brightness through centuries has been a mystery for scientists until the discoveries of new and sophisticated characterization techniques such as HRTEM, SEM, XRD, EELS, etc [17,19c]. With the help of these techniques, the Maya blue was found to be a hybrid organic-inorganic material with molecules of natural blue indigo encapsulated within the channels of a clay mineral known as palygroskite. It combines the colour of the organic pigment and the resistance of the inorganic host which show properties by far different from a simple mixture of the two [17].

The Maya blue resembles more the modern concept of hybrid materials. This modern concept of hybrid materials emerged recently with the research targeted to more sophisticated materials associated to development of composites and molecular materials where organic and inorganic components interact at molecular levels [19c, 20].

Figure 3: The Maya blue colour [17].

The earlier interest in the development of the hybrid materials was mainly focused on the design and improvement of polymeric materials with the emphasis of structural applications [21]. Various types of silicates, polysiloxanes, etc. modified with organic networks for improvement of mechanical properties were among the first hybrid materials investigated [19c, 21]. However, the importances of hybrid materials are not limited to this tiny application and many recent efforts open new fields in magnetic hybrids, electronic hybrids, optical hybrids, etc [19c].

2.2 Advantages of Hybrid materials

The possibility of combining organic and inorganic moieties in one material has numerous advantages. The first and most straight forward advantage is that the hybrid materials are creative [16, 17]. It is possible to combine the organic and inorganic phases in infinite ways and get a large number of materials. The properties of these materials could be within spectrum of known or unknown properties which are yet to be studied.

The second advantage of hybrid materials is the fact that it is possible to produce a multi-functionalized material. By doping organic inorganic hybrid materials with specific dopants for intended purposes, it is possible to functionalize a material. These dopants could be either inorganic or organic. For instance, doping organic inorganic hybrids with

lanthanide elements and different kinds of organic dyes has long been researched [16, 22, 23] and found applications in optics, electronics, displays, etc.

Thirdly, the hybrid materials are relatively easy to process: Hybrid materials are synthesised with a sol-gel route which is a relatively easy and cost effective synthesis method. Unlike solid sate inorganic materials which need high temperature treatment for their processing, hybrid materials show a more polymer-like handling, either because of the presence of organic components or because of formation of cross linked inorganic network from small molecular precursors just like polymerization reactions [16a]. Therefore, these materials can be shaped in any form in bulks and in films. With sol-gel synthesis route it is also possible to control the composition as well as the dimension of the constituents which helps to modify the properties of the hybrid materials. For instance, one can increase the hydrophobicity of materials by increasing the hydrophobic molecular components. Like wise by controlling the dimensions of the building blocks, it is possible to avoid light scattering in homogeneous hybrid materials and therefore increase optical transparency [16b]. The other advantage which can be considered here is the formation of smart materials which are sensitive to changing environments. For instance, sensors, membranes, biohybrids, etc. are some smart materials where the advantage hybrid material is considered. In organic-inorganic hybrids the desired function for smart materials can be derived from either the organic or inorganic or from both components [16b]. .

Moreover, the hybrid organic inorganic materials present an enormous amount of advantage to facilitate both miniaturization and integration in electronics and optical communications [23].

2.3 Applications of Hybrid materials

Even though the search of new materials in this field remains an endless task because of infinite number possibilities to design a material with a given property, the research on the organic inorganic hybrid materials has already gone beyond the academic interests of finding new materials. The improved and unusual features of the hybrid materials open promising applications in many areas: optics, electronics, ionics, mechanics, energy, biology, biotechnology, medicine, etc [21, 23].

The possible applications include: smart membranes and separation devices, functional smart coating, a new generation of photovoltaic and fuel cells, photo catalysts, smart mi-

croelectronics, micro-optical and photonic components and systems for nanophotonics, innovative cosmetics, intelligent therapeutic vectors that combine targeting, imaging, therapy and controlled release of active molecules, nanoceramic-polymer composites for automobile or packing industries, etc [23].

In particular, the application of hybrid materials for optical purposes such as integrated optics, displays, and light emitting devices has been very well developed [16b, 23]. Doping the hybrid materials with optically active centres like lanthanides and organic molecules add enormous values to the hybrid materials and increase their optical performances [17, 22, 24]. The incorporation of organic molecules, which is the focus of this work, into the organic-inorganic materials has played an important role in the development of optical systems. Luminescent solar concentrators, dye lasers, sensors, photochromic devices, non linear optical properties (NLO) and photovoltaic devices are some of the examples that can be considered [16b,17]. In this manner, the incorporation of organic dyes such as rhodamines, pyranines, spyrooxazines, chromenes, diarylethenes, courmarins, NLO dyes, etc. into silica or aluminosilicate based matrices, giving transparent films or monoliths with good mechanical integrity and excellent optical quality as illustrated in Figure 4 have already been reported [17].

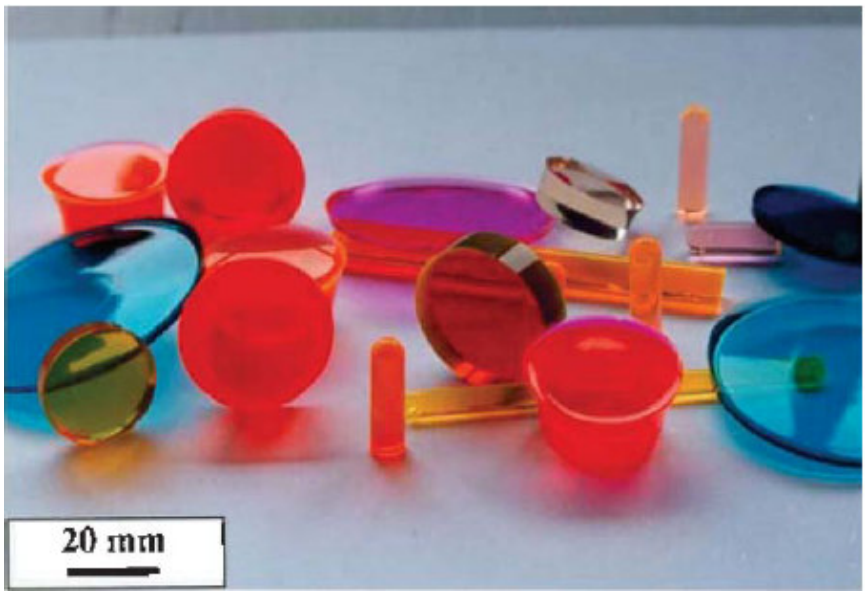

Figure 4: Hybrid organic inorganic materials doped with organic chromophores [17].

2.4 Types of hybrid materials

The classification of hybrid materials is very subjective from author to author in the area. Some of the factors which authors consider to classify the hybrid materials are: the types of interaction forces between the organic and inorganic components, the major constituent used in the synthesis of the material, and the synthesis route used. In this section we will consider and discuss some common ways of classifying the hybrid materials.

2.4.1 Hybrid materials by interaction forces: Class I & Class II

Depending on the interaction forces between the organic and inorganic moieties hybrid materials are classified in two broad groups [16-19]: class I and class II hybrid materials. Class I hybrid materials are materials in which the organic and inorganic components are mixed and only show weak interactions between them. The interactions could be van der Waals, hydrogen bonding or weak electrostatic interactions between the components which gives the cohesion to the whole structure [16-21]. Class II hybrid materials are those hybrid materials that exhibit strong chemical bonds between the two components. These interactions could be strong covalent bonds, iono-covalent bonds or coordination bonds between the moieties [16-19, 23]. Because of the gradual change in the chemical interaction between the two components there is a steady transition between the two classes of the hy-

brid materials, i.e. on the course of time class I hybrid may change to Class II. An illustrative scheme representing the different kinds of class I and Class II hybrids materials and the difference between them is shown in Figure 5.

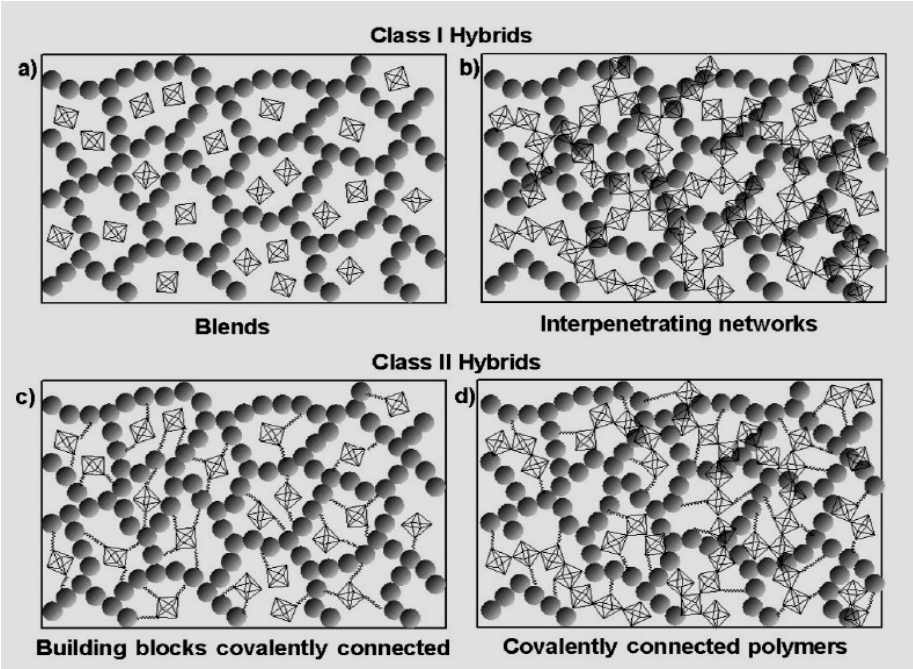

Figure 5: Class I and Class II hybrid materials [16a].

2.4.2 Hybrid materials by major component of the hybrid

The second classifying technique of the hybrid materials is depending on the variations of the major components of the hybrid materials [19a, 19c]. In this case, the hybrid materials are classified as Organic inorganic (OI), Inorganic organic (IO), and Nanocomposite. The Organic inorganic (OI) hybrid materials refer to the hybrid materials which have organic component as major constituents. Inorganic organic (IO) hybrid is the case where the roles of organic and inorganic constituents are interchanged or the inorganic quantity is higher than the organic part. However, Nanocomposite is the case in which neither of the components dominates but, both types of the components are dispersed at the nanometric scale.

2.4.3 Hybrid materials depending on their synthesis route

The third classifying technique of the hybrid materials is depending on their synthesis methods. Accordingly, hybrid materials are classified as: intercalation compound, organic derivative of inorganic solids and sol-gel hybrid materials [16b].

The intercalation compound refers to materials with guest molecule / atom inserted into the host system reversibly. For example, the insertion of organic dye (e.g. rhodamine 6G) into the interlayer of laponite clay is one among many possible hybrid materials in this class [12].

The organic derivatives of inorganic solids are the class of hybrid materials where the organic groups are made to react with the inorganic groups on the surface of the later. An example of this class of hybrid materials is the grafting of organosilane on to the surface of inorganic clays [18].

The sol-gel based hybrid material is the class of hybrid material which offers the largest scope of hybrid materials [16b]. Sol-gel is a soft chemistry synthesis technique used to fabricate materials ranging from macroscopic to nano-scale with the "bottom up" approach synthesis route. It mostly starts from metal alkoxide precursor and forms a material by undergoing two principal reactions: hydrolysis and condensation reactions. The next section of this work is devoted to the general overview of the sol-gel process: the reaction principles involved, catalysts necessary for the reaction, possible applications, etc.

Chapter 3: Sol-Gel process

Sol- gel is a wet chemical, low temperature, synthesis technique which is used to fabricate solid bulks, thin films and particles. It is a widely used technique in materials science engineering for fabrication of materials starting from a solution, sol, as a precursor and forming an integrated network, gel, of the material which could be either discrete particles or network of polymers [8, 25]. Using this method it is possible to coat on glass, ceramics, metal, and other solid substrates. Most importantly, its mild synthesis process opens new and easy ways to incorporate dopants such as organic dyes and /or metals which change the optical properties of the host, the dopant or both completely or modify to an extent [8, 25].

The use of this chemical route is well established. It relies on the versatility of silicon chemistry which bases on the remarkable stability of bonds between silicon-oxygen and silicon - carbon atoms. Furthermore, the sol-gel process has the following significant advantages over the solid chemistry processing routes: 1) High reactivity, purity, and homogeneity of the precursors; 2) the possibility of controlling the micro and macro structure of the host matrices; 3) the presence of a siliceous network, which provides simultaneously good mechanical resistance, extraordinary thermal stability, and amorphous character; 4) the possibility of grafting organic groups to the inorganic backbone at low processing temperatures; 5) possibility of preparing elastomeric transparent monoliths of variable thickness [26].

Materials for different specific applications such as optics, protective and porous films, optical coating, window insulator, dielectric and electric coating, high temperature superconductors, reinforcement fibers, fillers and catalysts can be produced by using this mild processing technique [27a]. The sol-gel process undergoes two main reaction steps to end up giving the desired products. Below is a discussion about the general reaction mechanisms that sol-gel process undergoes.

3.1 General description of sol-gel process

The sol-gel process is based on two consecutive reactions known as hydrolysis and condensation reactions of the precursors. The starting materials (precursors) could be an inorganic salt or metalorganic compounds [8, 25, 27]. The family of the latter compound,

namely, metal alkoxides are the widely used precursors in the sol-gel research. The most common metal alkoxide precursors are used to produce silicates, titania, germanates, alumina, zirconia, tungstates, vanadates, and ormosils [8].

Silicon alkoxide is a widely investigated precursor among metal alkoxides. They are generally represented as $Si(OR)_4$, where R is the alkyl group which could be represented by a general formula of C_xH_{2x+1} with x signifying the number of carbon atoms in the compound, and thus, OR is the alkoxy group.

Some of the examples of organoalkoxysilane molecules which are used for silicate sol-gel process are: tetramethoxysilane (TMOS) $Si(OCH_3)_4$, tetraethoxysilane (TEOS) ($Si(OCH_2CH_3)_4$), tetra-n-propoxysilane ($Si(n-OCH_2CH_2CH_3)_4$; tetra-n-butoxysilane $Si(n-OCH_2CH_2CH_2CH_3)_4$, etc [25]. Among these, TEOS is the most thoroughly studied silicon alkoxide. Therefore, one can use the TEOS as a model system to explain the general reaction principles in the sol-gel process. One of the importances of metal alkoxides (e.g. TEOS) for sol-gel process is the fact that they readily react with water. This reaction, known as hydrolysis process, occurs by the nucleophilic attack of the oxygen in water on the metal atom.

3.1.1 Hydrolysis

This is the initial stage of the sol-gel process. For the starting mixture which contains TEOS and water, the hydrolysis reaction has the following form:

$$Si(OR)_4 + H_2O \underset{esterification}{\overset{Hydrolysis}{\rightleftharpoons}} HO-Si(OR)_3 + ROH \quad \text{..... (1)}$$

If the TEOS undergoes complete hydrolysis, then the final product of the hydrolysis reaction will be a solution of silanol group, $Si(OH)_4$ i.e.

$$nSi(OR)_4 + 4nH_2O \underset{esterification}{\overset{hydrolysis}{\rightleftharpoons}} nSi(OH)_4 + 4nROH \quad \text{..... (2)}$$

Any intermediate species such as $(OR)_2Si(OH)_2$, $(OR)_3SiOH$ and $(OR)Si(OH)_3$ are considered as a result of the partial hydrolysis.

3.1.2 Condensation

The second stage of sol-gel process is the condensation reaction of the hydrolysis products. Similar to the organic polycondensation reaction, monomers which are the output of hydrolysis stage react to form large polymers by liberating small molecules like water or alcohol [8, 25, 27]. The end product of hydrolysis, partial or complete, reaction of the TEOS is an unstable silanol species which are formed by replacing the alkoxy group (OR) with the hydroxyl group (OH). These silanols subsequently condensate and form a siloxane $(-Si-O-Si-)$ bond along with the small by-products. If one considers two partially hydrolysed molecules, then the molecules link to each other and form siloxane bonds as in one of the following reactions:

$$(OR)_3-Si-OH+HO-Si-(OR)_3 \underset{hydrolysis}{\overset{H_2O-condensation}{\rightleftharpoons}} (OR)_3-Si-O-Si-(OR)_3+HOH$$

….. (3)

Or

$$(OR)_3-Si-OR+HO-Si-(OR)_3 \underset{alcoholsis}{\overset{alcohol\_condensation}{\rightleftharpoons}} (OR)_3-Si-O-Si-(OR)_3+ROH$$

….. (4)

The condensation process which gives H_2O (eq.3) as an output is know as water condensation whereas the one with alcohol (eq. 4) output is called alcohol condensation. If it happens that the condensation reaction proceeds only after the hydrolysis is complete, so that all the reactants are silanols, then the general form which describes polycondensation stage is given by:

$$nSi(OH)_4 \xrightarrow{H_2Ocondensation} (SiO_2)_n + 2nH_2O \quad \text{…….. (5)}$$

The results of condensation reaction are the formation of dimers, linear or cyclic trimers, tetramers, rings, oligomers, and eventually 3D cross linked polymer networks leading to the formation of sol. A further condensation reaction links the sol particles and forms a wet gel [16a, 25]. This is the transition point from sol to gel and is known as gelation point. At this point the reaction is not over, but condensation proceeds until the final result is reached. This process is known as ageing. Next to ageing, drying step in which the further condensation reaction proceed follows. While drying, trapped volatile molecules (water, alcohol, etc.) are driven off and the network shrinks as further condensation occurs. Dur-

ing the process of drying cracking is the main problem. This is due to the large capillary force of the evaporating liquid through the porous structure leading to the cracking of the materials. Firing is the step which might follow depending on what kind of density the final product must have.

Equations 1, 3, and 4 which represent sequentially the hydrolysis and condensation reactions together with the reverse processes such as esterification (eq.1), alcoholic and hydrolytic depolymerizations (eqs. 3 and 4) are the main reaction steps involved in sol-gel processes. As the final structure of the sol-gel product depends on these basic reactions, the important concern should be on controlling chemical and physical factors that affect the sequence of these reactions precisely. Reaction temperature and time, pH, reagent concentration, nature of catalyst and concentration, the ratio of water to silicon atom, ageing temperature and time, and drying are some of the well documented factors which affect the hydrolysis and condensation reaction in sol-gel process. Most importantly, pH, type and concentration of catalyst, water to silicon atom ratio, and temperature have been identified as the crucial factors and therefore, need to be fine-tuned to control the final structure and properties of the sol-gel derived materials [21].

The hydrolysis reaction with water is a very slow process. As a result of this, subsequent condensation reaction which involves silanol groups to produce siloxane bonds begins before hydrolysis ends. This can be overcome using reaction conditions mentioned above such as pH, catalyst, and H_2O to silicon ratio. In addition to this the immiscibility of alkoxide in water is also one of the factors which hinders the completion of the hydrolysis reaction fast. Usually solvents such as alcohol and acetone [8, 25] are used as a mutual solvent, to homogenize the solution and facilitate the reaction. These solvents, however, can also interfere with the hydrolysis process and reverse reaction by the process of esterification (eq.1) may occur.

Hydrolysis reaction can be catalysed either by an acid via electrophilic mechanism or basic catalysts via nucleophilic mechanism. The reaction rate of hydrolysis is increased with the strength of the acid. Besides, HCl, HNO_3, KOH, NaOH are some of examples of the acidic and basic catalysts used in a hydrolysis process. The hydrolysis reaction is also affected by steric hindrance and decrease with the increase of the alkoxy group. Thus, the TEOS is less hydrolysed than TMOS [8, 25].

The type of the network structure formed in the sol-gel process depends on the number of bonds (functionalities) that the monomers can form in the reactions. Monomers with a single functionality will only react with one molecule. Monomers with two functionalities react with two other monomers and form a polymer of linear chain or ring type network. However, monomers with functionality greater than two can form cross links to form a three dimensional structure [25, 27b].

The functionality or the number of reactive hydroxyl group of the TEOS monomer depends on the amount of the hydrolysing molecules (e.g. H_2O). If as much molecule of water as needed by the precursor is used in the hydrolysis process then a single molecule of silanol formed will have four functionalities. Thus, under this ideal condition the condensation process forms a 3D network of solid polymer. In TEOS the functionality of the monomer, sol, ranges from zero to four depending on whether there is no hydrolysis to the condition where there is complete hydrolysis. Thus the possible network that can be formed ranges from absence of the final results to the formation a three dimensional network. For instance, for TMOS precursor, any of the following possible networks, as shown in the schematic diagram (Figure 6) [25], can be formed depending on the functionality of the sol. Thus, the amount of water used in the reaction is one of the major factors affecting the final product in the sol-gel process [16a] for non-catalyzed reactions.

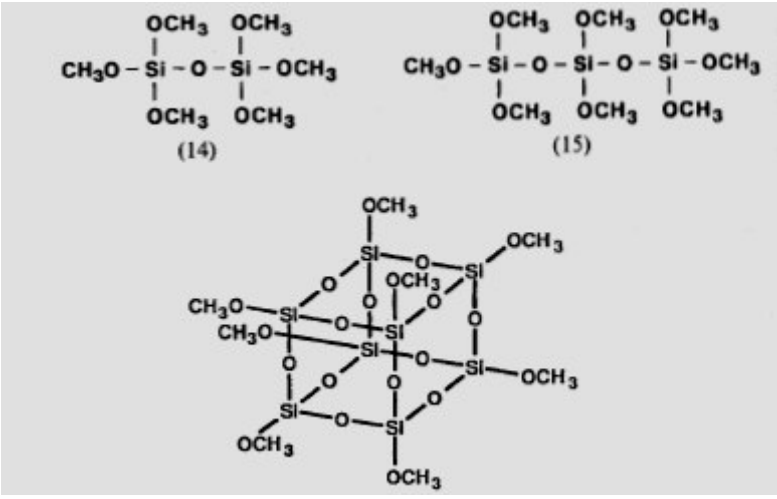

Figure 6: The possible networks of siloxane [25].

Similar with the hydrolysis, condensation can proceed withoutthe presence of catalyst; however, their use in the reaction is highly beneficial. For instance, polycondensation reac-

tion can be catalysed by hydrofluoric acid, HF, since F^- ion can replace the hydroxyl ion in the hydrolysis product, $Si(OH)_4$, and being more electronegative than the hydroxyl, they increase the attraction to other silanols leading to the siloxane bonds. Polycondensation can be catalysed by base as well. The use of catalyst not only affects the reaction mechanism but also the microstructure of the final materials. Applying acid catalyst to the reaction leads to the formation of an open network structure. Contrarily, the base catalysed reaction leads to the formation of a highly cross linked structure. Figure **7** [27a] shows the schematic diagram representing the structures of acid and base catalysed final materials.

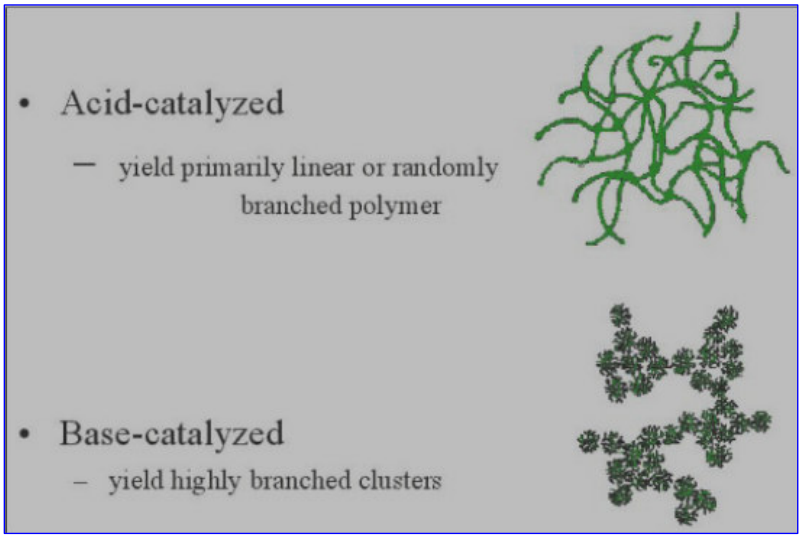

Figure 7: Acid and base catalysed materials [27a].

After the reaction is complete to give sol, it can be used in different way to fabricate different materials. It can be deposited on a substrate to form a thin film either by dip coating or spin coating, cast into a suitable mold with desired shape (to obtain monolithic ceramics, glass, fibers membranes, aerogels), or used to synthesize powders with a spherical shapes. The diagram given in Figure 8 shows schematically the different possible routes through which sol can be used to fabricate different materials.

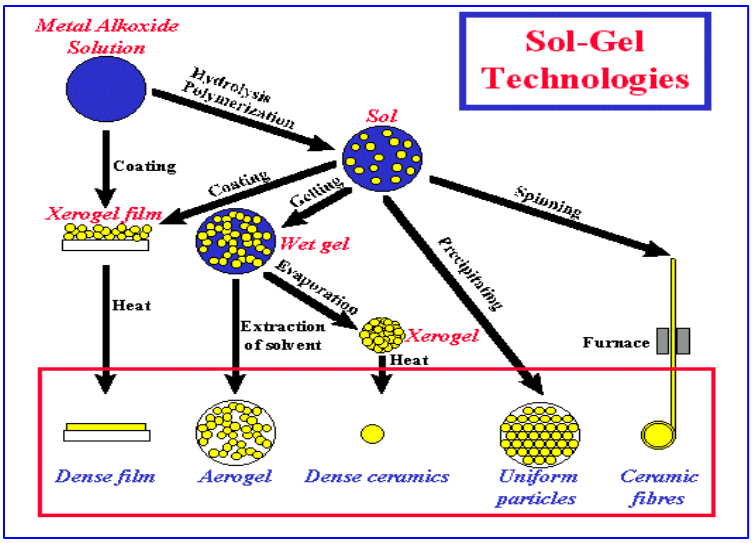

Figure 8: Possible products after sol is produced [27c].

3.2 Amine functionalized hybrid materials

In recent years, the concept of hybrid is employed to a sol-gel derived amine functionalized organic-inorganic hybrid materials. These hybrid materials essentially involve four alkoxysilane precursors. These are 3-isocyanatopropyltriethoxysilane (ICPTES), 3-glycidyloxypropyltriethoxysilane (GPTES), 3-glycidyloxypropyltriemethoxysilane (GPTMS), 3-aminopropyltriethoxysilane (APTES) [28]. Urea, urethane, and di-amide cross linked hybrids classed as di- ureasils, di-urethanesils, and di-amidosils are among the amine functionalized hybrid organic-inorganic materials [26, 28-32].

These hybrid materials consist of siliceous skeleton to which oligopolyether chains of different lengths are covalently grafted by means of urea [26, 30, 31], urethane [28], and di-amide [29]. The optical property of these hybrids has widely been studied and shown that they are characterized by broad emission spectra which give full colour (white emission). For instance, the diagrams shown below indicate a model structure of the hybrid material showing the siliceous clusters embedded in polymer matrices and the emission property of a di-ureasil hybrid material with white light seen in the inset of the figure [32].

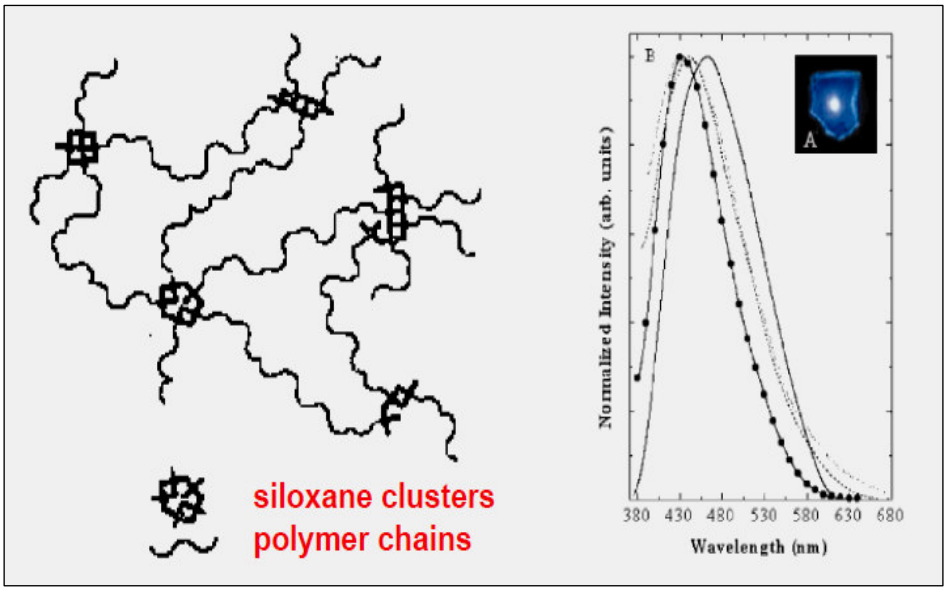

Figure 9: Siloxane clusters and polyoxyethylene units linked by urea brides- UREASIL (left diagram), the full colour emission of the di-ureasil hybrid (right diagram) [32].

In this work, the same di-ureasil hybrid material is used as a host for the organic dye. This di-ureasil hybrid material is one of the ranges of di-ureasil hybrid materials which is known for its optimized optical properties [26, 28, 31, 32]. The interaction between the organic dopants and the emitting centers of this di-ureasil changes the optical properties of both the host and guest moieties. As a result the main targets of this work are to figure out the change in optical behaviours of the di-ureasil and the dye by varying the concentration of the organic dyes and study the structural features of the material. In order to study these optical and structural properties of the materials we employ absorption, photolumines-cence, and X-ray diffraction techniques. In the next section we will consider and discuss the theoretical principles of these characterisation techniques.

Chapter 4: Characterization of hybrid materials

In relation with the versatility of the organic inorganic hybrid materials, there are various characterizing techniques which are used to analyse the chemical, physical and structural properties of hybrid materials. Some of these techniques are: scanning electron microscopy (SEM), transmission electron microscopy (TEM), optical microscopy, X-ray diffraction (XRD), small angle X-ray scattering (SAXS), atomic force microscopy (AFM), photoluminescence (PL), absorption, thermal analysis (TGA and DSC), nuclear magnetic resonance (NMR), etc [16a, 33]. Among these techniques, we use XRD, absorption and photoluminescence characterization techniques to characterize the optical and structural properties of the organic dye doped into the hybrid materials. In this chapter we shall focus on discussing the theoretical background of these techniques.

4.1 Absorption

When an atom or a molecule absorbs energy, electrons are promoted from their ground state to an excited state. In molecules the atoms can rotate and vibrate with respect to each other. These vibrations and rotations have discrete energy levels, which can be considered as being packed on top of each electronic state [34, 35a]. The schematic diagram given in Figure 10 shows the arrangement of the energy levels of vibration, rotation and electronic states.

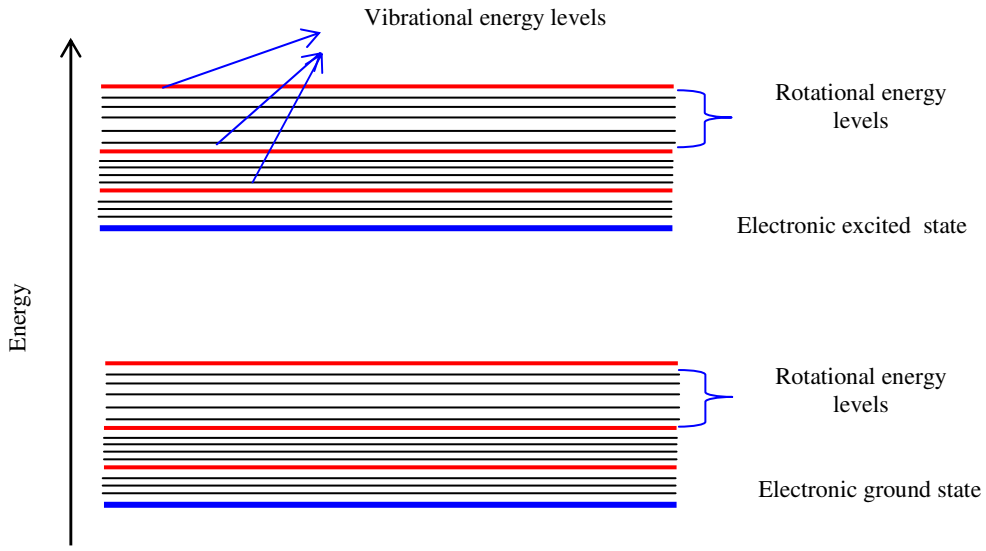

Figure 10: Energy levels of a molecule.

In absorption spectroscopy a photon must match the energy gap between the higher and lower energy levels to be absorbed. For instance, the excitation of outer electrons corresponds to the absorption of UV or Visible radiation.

The spectra from molecules are more complex than atomic spectra and convey richer information. The greater complexity arises from the more complicated structures of molecules. The spectra of atoms are only due to their electronic transitions. In contrast, the spectra of molecules arise from electronic, vibrational and rotational transitions. These transitions are not independent of each other, and the complexity of the spectrum is enhanced by them. The energy associated with rotational transitions is usually less than vibrational transitions, and the energy associated with vibrational transitions is less than electronic transitions. Therefore, although it's possible to observe pure rotational transitions without the interference from the others, a vibrational transition is accompanied by rotational transitions, and electronic transitions are accompanied by both vibrational and rotational transitions and are correspondingly more complicated [35a]. As a result of this, the spectrum of molecules contains superposition of the rotational and vibrational transitions on electronic transitions and gives a combination of overlapping lines. This appears as a continuous absorption band unlike discrete absorption lines in atomic spectra. The interpretation of the molecular spectra yields a great deal of information about the shapes and sizes of molecules, the strength and stiffness of their bonds, the association levels of molecules, and other information that is needed to account for in a chemical reaction [34].

There are three types of electronic transitions that may involve in an absorption process. These are transition which involves bonding (σ and π electrons) and non bonding (*n-electrons),* transitions involving charge transfer electrons, and transitions involving *d* and *f* electrons [34, 35b]. The transitions involving charge transfer mostly occurs in an inorganic species and they are called charge transfer complexes. For a complex to show charge transfer property there should be two components with one of them having charge donating property and the other one charge accepting property. The transition involving the *d* and *f* electrons play roles in the absorption processes of transition metals (*d*-electrons) and rare earth elements (Lanthanides and Actinides) (*f*-electrons). In organic molecules, absorbance depends on some functional groups (chromophores) that contain valance electrons.

The possible electronic transition involves transitions between bonding or nonbonding states and anti-boding states [34, 35]. The schematic diagram given in Figure 11 shows the possible transitions between the bonding, nonbonding and anti-bonding states.

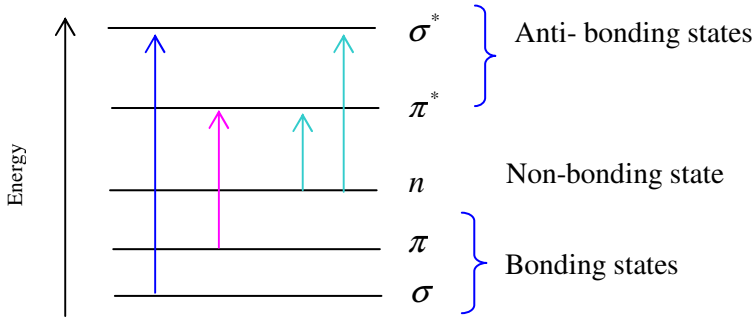

Figure 11: The possible electronic transitions.

Experimentally, the consequence of absorption is that the beam of light passing through an absorbing medium is attenuated. This attenuation of beam can be described quantitatively by the so-called Beer-Lambert law which is a linear relationship between an absorbance *A*, number density of an absorbing quantity, *N* and a path length, *l*. Considering a diagram given in Figure 12 showing the general attenuation principles, one can write the Beer-Lambert law as [35],

$$A = \varepsilon N l \equiv \alpha l \quad \ldots\ldots\ldots \quad (4.1)$$

where *A* (dimensionless) is the measured absorbance, ε (cm^2) is the absorption coefficient, *N*(cm^{-3}) is the analyte particle density, *l* (cm) is the path length, and α (cm^{-1}) is the attenuation coefficient. Since experimental measurements are usually made in terms of transmittance, T, which is defined as

$$T = I/I_0 \quad , \ldots\ldots\ldots\ldots\ldots\ldots\ldots\ldots \quad (4.2)$$

where *I* is the intensity of the beam after it has passed through the sample and I_0 is the intensity before it enters the sample, absorbance can be written as

$$A = -\ln(T) = \ln\left(I_0/I\right). \quad \ldots\ldots\ldots\ldots\ldots \quad (4.3)$$

Combining equations (4.1) and (4.2) the intensity of the out going beam can be related to the incoming beam by a decay type equation as

$$I(\lambda) = I_0 \exp(-\varepsilon(\lambda)Nl) = I_0 \exp(-\alpha l) \,. \ldots\ldots\ldots\ldots \quad (4.4)$$

Therefore, by measuring the intensities of beam before and after the sample it is possible to calculate the unknown parameters. However, for high concentration, Beer-Lambert law fells to work.

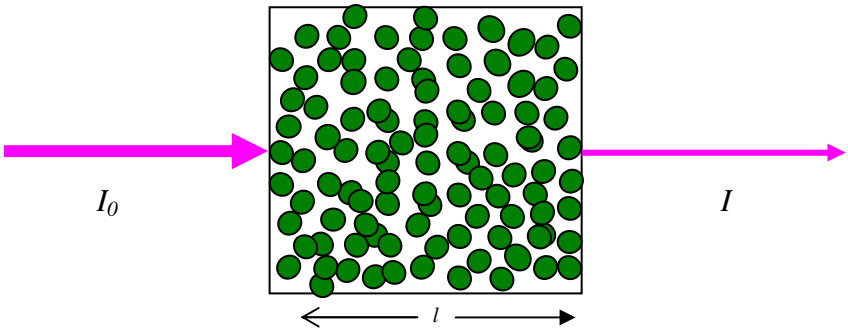

Figure 12: schematic representation of absorbing molecules with incoming and outgoing beam of light.

4.2. Photoluminescence processes

Luminescence is the emission of light by a substance through any process other than thermal or black body radiation [16a]. It occurs when a molecule or atom in the excited state returns to the fundamental state by giving its energy in the form of photon. Luminescence spectroscopy is a collective name given to three spectroscopic techniques which are very close to each other. These techniques are molecular fluorescence, molecular phosphorescence and chemiluminescence. They differ from each other by the excitation sources which are used to excite the molecules from their ground state. The excitation source of the first two luminescence spectroscopy is light or photon. As a result of this, they together are called photoluminescence processes. However, the excitation source for the later luminescence process is a chemical reaction which excites the electron to a higher energy level.

The difference between fluorescence and phosphorescence lies on spin multiplicity of the electronic energy levels of the molecules. In quantum mechanics, the molecular electronic energy levels are divided into two categories: the electronic singlet and triplet states. In the electronic singlet state, the electrons in the molecules are spin paired. The resultant spin in the system is therefore zero (**s**=0) and restricts the possible values of the quantum number m_s to be zero as well [35a, 36]. If, however, one set of the electron spin is unpaired then the

resultant spin becomes $\hbar$ where, $\hbar (=1.055\times10^{-34} Js)$ represents the reduced Planks constant. Unlike the singlet state, the quantum number, $m_{s,}$ has three possible values; namely, -1, 0, and 1. As a result of these differences, the spin state which corresponds to the total spin $\hbar$ is known as triplet state whereas the one that corresponds to the resultant spin of 0 is called the singlet state. Therefore, if the transition of the excited electron happens to be from the excited singlet state to the ground state then the process is known as fluorescence. However, if the transition is from the excited triplet state to the fundamental state then the process is known as phosphorescence [35a, 36]. They can also be identified by the time scale in which the processes may happen. In the fluorescence (10^{-8} sec) process, the emission of light ends soon after the excitation source is taken off. However, in phosphorescence (1ms-1sec or even more) it takes a while to decay to zero value after the source is removed [36].

Apart from these two processes, there are other energy release mechanisms by which a molecule excited to high energy levels returns to the fundamental state. Vibration relaxation, intersystem crossing, internal conversion, etc. are among the mechanisms. To have a general picture of the possible physical processes that may happen following absorption by a molecule let's consider the diagram shown in Figure 13. This diagram is known as Jablonski diagram named after the Polish physicist, Aleksander Jablonski. It is a convenient diagram to visualize the possible physical processes involving photon absorption and de-activation of the absorbed energy.

4.2.1 Fluorescence, Vibrational relaxation, and internal conversion

Absorption of the photon by a molecule excites it from a vibrational level in the electronic ground state to any of the possible vibrational levels of excited electronic states depending on the absorbed photon. These excited states are usually the electronic singlet states (say S_2). This is because of the selection rule which does not allow absorption which involves the change of spin state ($\Delta s = 0$) [35a]. The molecule at the higher vibrational level of the excited singlet state quickly returns back to the lowest vibrational level of the same state (S_2). It does this by releasing its energy in the form of heat while colliding with the rest of the molecules. This process is known as vibrational relaxation (~10^{-12}sec.) [36, 37]. After the molecule reaches the lowest vibrational states of the same singlet state (S_2), it can do two things. The first one is that the molecule may release its energy in the form of photon

and returns back to one of the vibrational states of the electronic ground state (S_0). This process is termed as fluorescence (~10^{-8}sec.). The second possibility is that the molecule may release its energy non radiatively and makes transition from that lowest vibrtational level (of S_2) to one of the vibrational levels of another excited singlet state (S_1) or electronic ground singlet state (S_0). This process is known as internal conversion (IC). If the transition is to one of the vibrational levels of the ground electronic singlet state, then the molecule relaxes vibrationally to the ground state. However, if the transition is to one of the vibrational levels of another excited singlet state (S_1), then the molecule makes transition to the lowest energy levels of this singlet states by vibrational relaxation. From this vibrational state fluorescence or internal conversion process may follow. The conversion of electronic energy to vibrational energy by internal conversion process is facilitated if the molecule is freely movable and allows the molecule to reorient itself in a way which aid internal transfer of energy.

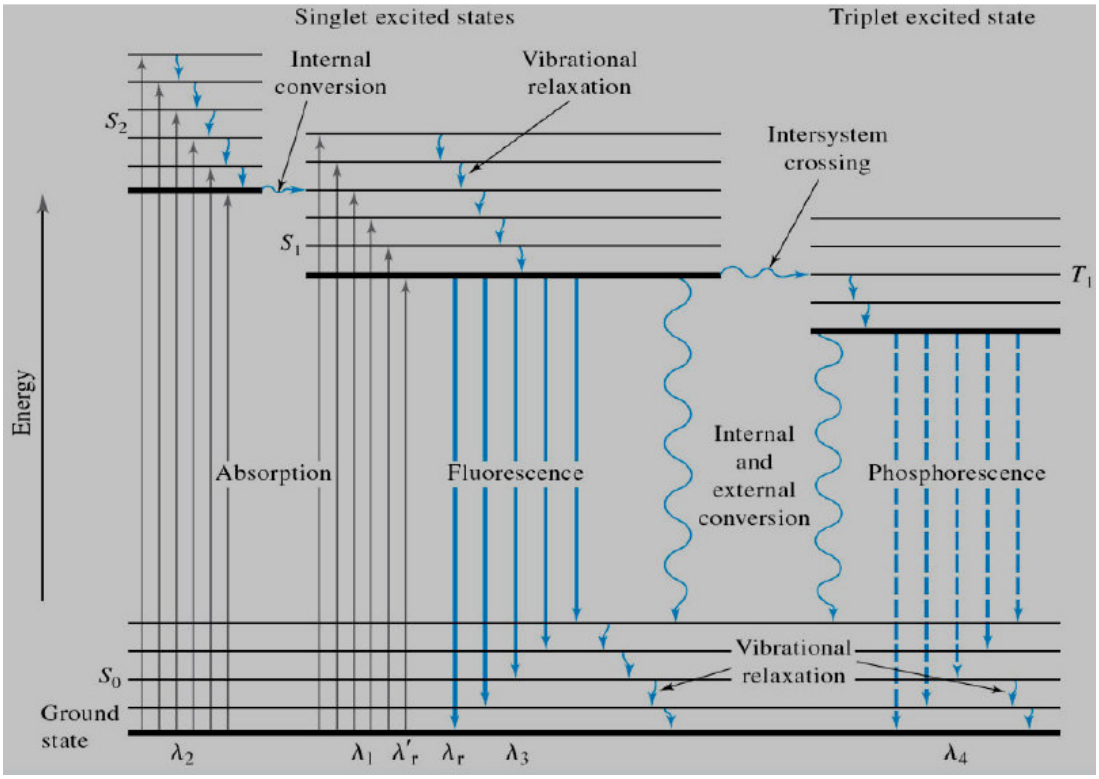

Figure 13: Jabloniski diagram [37].

4.2.2 Phosphorescence and Intersystem crossing (ISC)

So far the discussion was limited to the singlet-singlet electronic transitions. However, if the spin of the excited electron is inverted, then the molecule is said to be in a triplet excited state. Unlike the singlet state it is not possible to populate the triplet state directly from the ground state. Yet, there is an efficient mechanism by which the population of this state is effective; the intersystem crossing process (10^{-7}-10^{-9}sec) [36]. It involves non radiative transition from a singlet state to a triplet state. The probability of this happening is increased if the vibrational levels of these two states overlap. This condition is known vibrational coupling between the singlet state and the triplet state.

Once in a triplet state, the molecule undergoes the usual processes to return back to the vibrational levels of fundamental state. A molecule in a higher vibrational level of the triplet state can lose its energy by collision, vibrational relaxation, and leaves it in the lowest vibrational level of the triplet state. From this level it can return back to the ground state by a non radiative mechanism, internal conversion. Apart from this, there is also a possibility of returning back to the ground state by emitting photon. This process is known as phosphorescence. The radiative life time of phosphorescence is large (seconds to hours) as compared to the fluorescence life time.

In general, luminescence is the result of the competition of radiative and nonradiative pathways in the relaxation of an electronically excited molecule (entity). Because of the non radiative de-activation routes, it is customary that the fluorescence occurs at lower energy (longer wavelengths) than the exciting or absorbed photon. This energy difference between the maximum of the absorption band and maximum of emission band is known as the Stokes shift [36]. It is usually expressed in terms of wavenumber. The schematic representation of Stokes shift is indicated in Figure 14. The parameters shown in the figure, $\lambda_{abs}^{\max}$ and $\lambda_{ems}^{\max}$ indicate the maxima of the absorption and emission bands. Whereas, $\bar{\upsilon}_{abs}$ and $\bar{\upsilon}_{ems}$ indicate the wave number corresponding to the maximum absorbance and emission bands, and $\Delta\bar{\upsilon}$ represents the energy difference (Stokes shift).

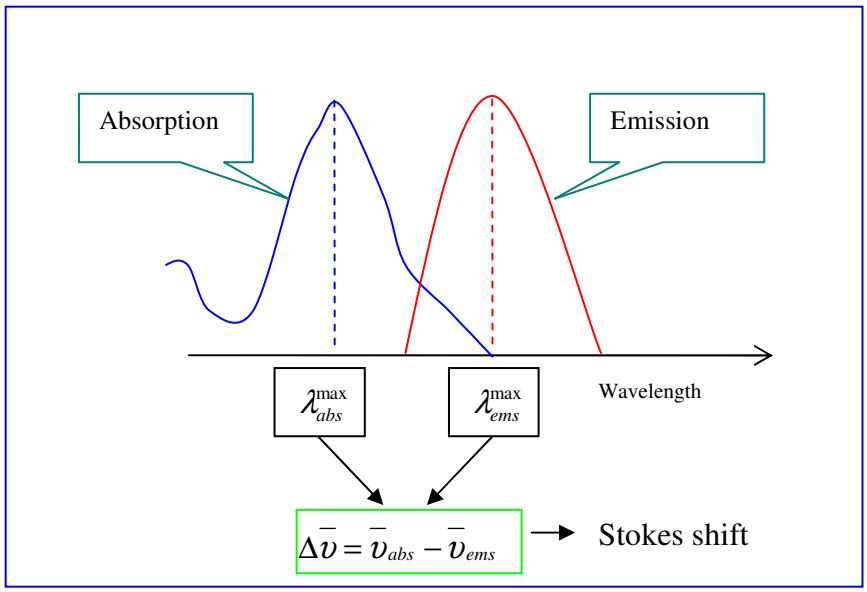

Figure 14: schematic representation of Stokes shift.

4.2.3 Fluorescence spectroscopy

In experiment, fluorescence spectroscopy uses a continuum light (excitation) source. However, instead of irradiating the sample with all the wavelengths a monochromator is used to select a single exciting wavelength. This allows only a single excitation transition to occur, and minimizes the interference which arises from the scattering of other wavelengths while detecting the emitted wavelengths. Selecting the wavelength with monochromator is performed two times in the instrument of fluorescence spectroscopy. The first one is performed by the monocromator just next to the excitation source. After the light interacts with the sample, the emitted wavelengths are also selected by a monochromator next to the sample cell. Technically, the first monochromator is known as excitation monochromator while the second one is named as emission monochromator. After exciting the sample with the wavelength selected by the excitation monochromator, the emission monochromator scans (usually starting 15-20 nm higher than the excitation wavelength) and records intensity at each emitted wavelength. This spectrum is known as emission spectrum. The converse of this process can also be performed and the spectrum is known as excitation spectrum. In this case, the emission monochromator is monitored at a fixed wavelength and the excitation monochromator scans (usually 15-20 nm lower than the monitored emission wavelength) and records intensity at each exciting wavelength which are responsible for the monitored wavelength. The luminescence spectra with a continuous excitation source

are known as steady state photoluminescence. However, it is also possible to measure the luminescence properties of a sample by using discrete light sources. This is known as time resolved photoluminescence. It involves a pulsed excitation source and requires spectral detection takes place after a certain time interval next to the excitation pulse. It is useful to study a dynamical evolution of processes after emission occur [16a].

4.3 X-ray powder diffraction (XRD)

X-ray diffraction (XRD) is one of the most powerful techniques for qualitative and quantitative analysis of the crystalline materials. The information obtained include type and nature of crystalline phases present, structural makeup of phases, degree of crystallinity and amount of amorphous content, micro strain, size and orientation of crystallites [33]. When a material is irradiated with a parallel beam of monochromatic X-rays, the atomic lattice of the sample acts as a three dimensional diffraction grating causing the X-ray beam to be diffracted at specific angles. The diffraction pattern, that includes position (in angles) and intensities of the diffracted beam, provides several types of information about the sample. The XRD beam diffracted from a material is in accordance with Bragg's law [33] which is given by

$$2d\sin(\theta) = m\lambda, \ldots\ldots\ldots\ldots\ldots\ldots \quad (4.5)$$

where d is an interplanar spacing, λ the X-ray wavelength, θ the Bragg's angle, and m indicates the order of diffraction.

Chapter 5: Experimental section

In this section the description of the synthesis steps taken to prepare the sample is presented without going to the detailed chemistry of the process. In addition, the measurement techniques used in general and diagrammatical description of the photoluminescence in particular are presented.

5.1 Synthesis

Materials

α, ω - Bis (2-aminopropyl) polypropylene glycol-block-polyethylene glycol-block-polypropylene glycol (Fluka), commercially known as Jeffamine ED-600 with average molecular weight of 600g/mol, tetrahydrofuran (THF) P.A. (stabilized - Riedel-de Haen), 3-isocyanatopropyltriethoxysilane (ICPTES, Aldrich 95%), Ethyl alcohol absolute P.A. (Carlo Erba), hydrochloric acid (HCl, ACS Reagent 37% - Sigma-Aldrich), rhodamine 6G hydrochloride 95% (Sigma), rhodamine B hydrochloride 95% (Sigma).

Step1: Preparation of di-ureapropyltriethoxysilane (d-UPTES)

Jeffamine ED-600 and (3-isocyanatopropyl) triethoxysilane (ICPTES) were mixed in a tetrahydrofuran (THF) which is a common solvent for both ICPTES and Jeffamine. The mixture was stirred by a magnetic stirrer rotating at 800rpm. The order of mixing these compounds into a flask was done as shown diagrammatically in Figure 15A.

To make the reaction complete, the flask containing the mixture was put in a silicon oil bath container which was kept on a hot plate at a temperature of 82 ºC (see Figure 15A). But, as the boiling point of THF is about 66 ºC the THF is found in vapour state at 82ºC used here. The flask of the mixture was then connected to a Graham type condenser which cools down the vapour form of THF and then returns it down to the reaction medium drop by drop. This process is called reflux.

In the reaction, the isocyanate group of the alkoxysilane precursor (ICPTES) reacts with the terminal amine groups of a doubly functional diamine Jeffamine ED-600 to form a urea cross linked hybrid organic-inorganic precursor called di-ureapropyltriethoxysilane (d-UPTES). This reaction is an addition reaction which involves two molecules of ICPTES for each of Jeffamine molecules. The flask with the mixture of d-UPTES and THF pro-

duced was rotated by rotary evaporator in a water bath heated at 50 ºC to allow extraction of THF under vacuum. The extraction process was continued until the solution became highly viscous. The schematic representation showing the extraction process is shown in Figure 15B. After extraction of THF, a transparent viscous liquid (d-UPTES) which is an organic/inorganic precursor for the formation of di-ureasils hybrid material was obtained.

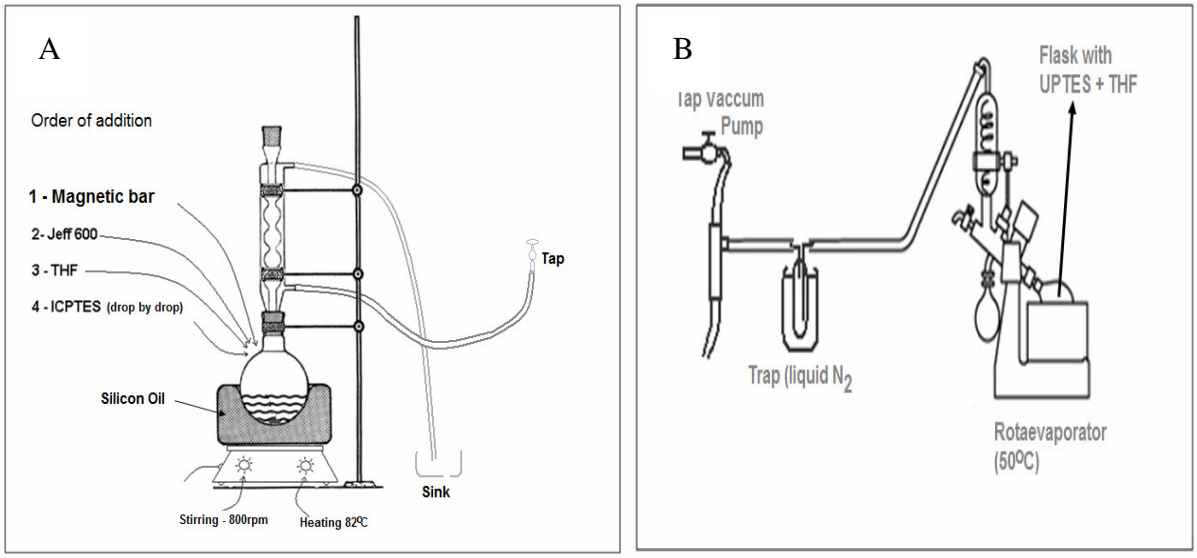

Figure 15: d-UPTES synthesis apparatus. A) Order of mixing components to produce d-UPTES. B) THF extraction.

Step2: Doping of the dyes with the d-UPTES

Keeping the d-UPTES under stirring condition, the powders of laser dyes, either Rhodamine B or Rhodamine 6G salts mixed in an ethanol solvent were added to the d-UPTES solution. The Rhodamine concentrations were based on molar% of silicon atom in the d-UPTES. In this way, the Rhodamines (B and 6G) concentrations equal to 0.008%, 0.1%, 0.2%, 0.3%, 0.4%, 0.8% of silicon atom in d-UPTES were calculated and used for doping. After the dye of appropriate concentration was mixed with d-UPTES, the usual sol-gel processes, hydrolysis and condensation, were followed. Moreover, as the Jeffamine is an amine functionalized polymer, it behaves as an organic base with pH around 9-10. This character of the Jeffamine guarantees the hydrolysis process possible without the supply of

water. To push the pH of the solutions to a more acidic region and make the gelation fast enough, HCl (2M) was used.

Before gelation starts the solution was poured to a mold and kept at room temperature for 48hours. This is the ageing stage. Then the gel in the mold was put in an oven at 40ºC for 48hours, 60ºC for 48hours and 70ºC for 12 hours sequentially to advance drying of the sample. These step by step putting of the gel in an oven at different temperature were to avoid cracking while the solvent was removed from the sample. In this manner a solid organic-inorganic hybrid materials doped with rhodamine dyes of different concentrations were prepared. The schematic representation showing the whole synthesis process of the sample is given on the next page:

Scheme1: Schematic representation of the synthesis of the d-UPTES and doping of d-UPTES with dyes

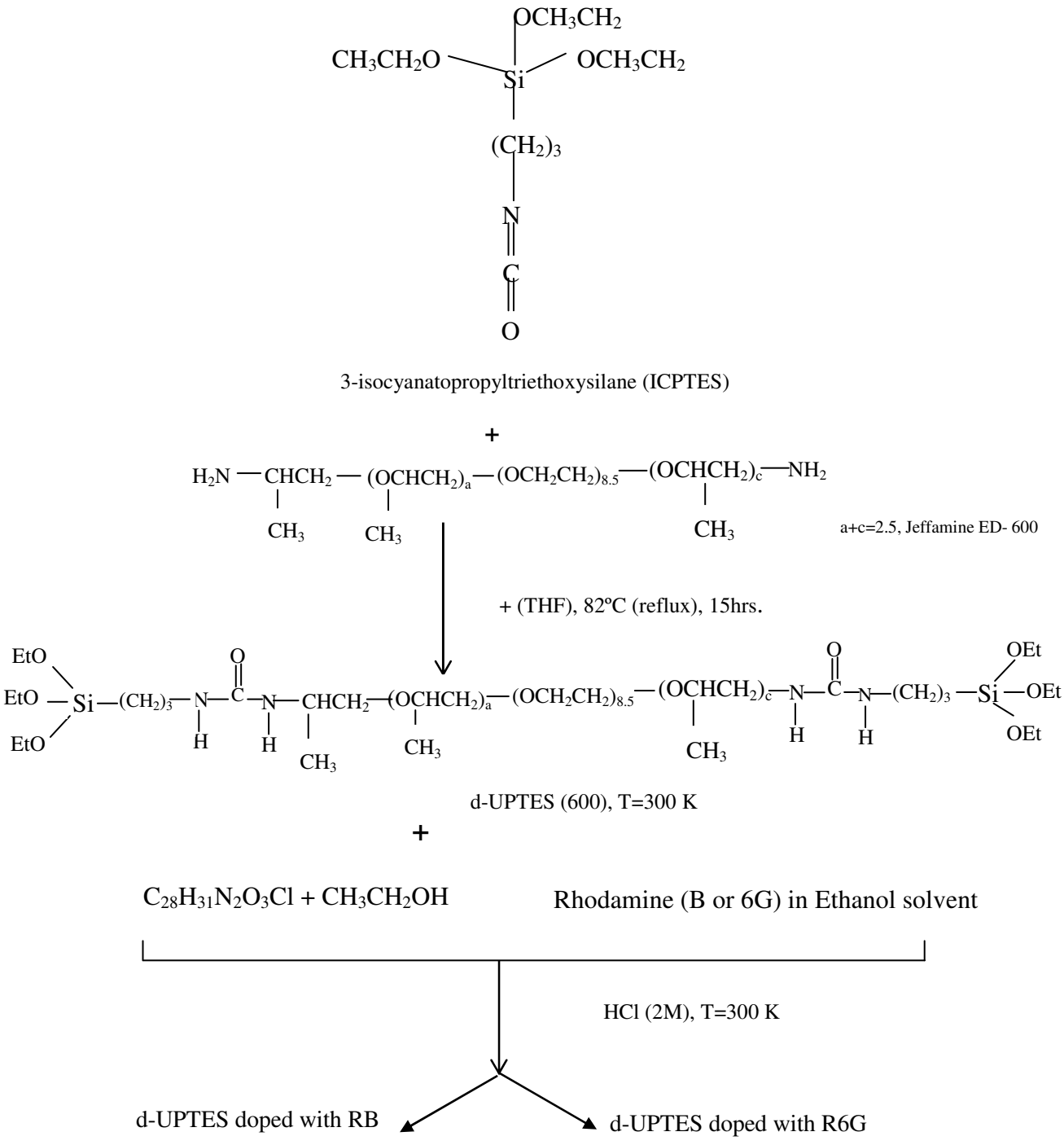

5.2 Measurement techniques

Absorption:

The absorption spectra of both rhodamine B and 6G doped samples were measured by a double-beam spectrophotometer (model Jasco V-560) in diffuse reflectance method within a wavelength range between 250-850 nm.

X-ray diffraction (XRD):

Powder diffraction (XRD) patterns were recorded on a Philips X'pert MPD diffractometer, using Cu Kα radiation of wavelength 1.54A° between 1° and 70° (2θ).

Photoluminescence Spectroscopy:

The steady state photoluminescence (emission and excitation spectra) of the samples were obtained at temperatures of 12 K and 300 K and recorded by a double modular-grating excitation spectrofluorimeter (with a linear dispersion of 2.1 nm/mm and 1200 grooves/mm) with a TRIAX 320 emission monochromator (with a linear dispersion of 2.64 nm/mm and 600 grooves/mm) coupled to R928 Hamamatsu photomultiplier (Fluorolog-3, Jobin Yvon-Spex).

The spectrofluorimeter used to measure the steady state photoluminescence spectrum basically consists of elements shown in Figure 16; namely: 450 W Xenon lamp excitation source, excitation monochromator, sample holder, emission monochromator and detector (R928 Hamamatsu photomultiplier).

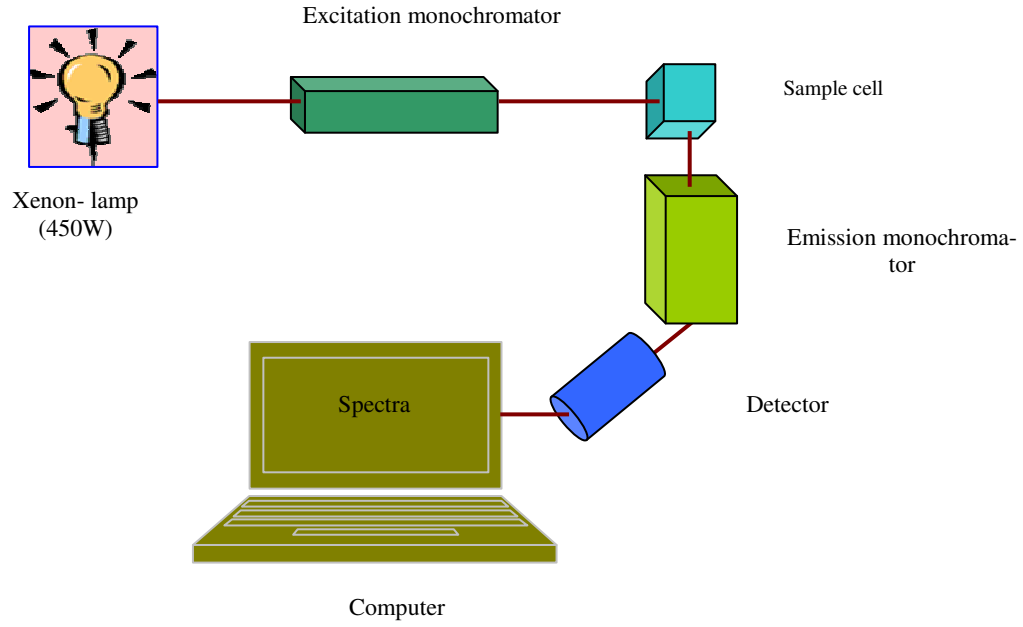

Figure 16: Schematic representation of the spectrofluorimeter layout.

Emission spectra were acquired by exciting the samples with the required energy and scanning the luminescence on the interval of interest with emission monochromator. Likewise, excitation spectra were recorded by monitoring emission wavelength fixed at a given value and then scan the luminescence with excitation monochromator on a given range to acquire luminescence intensity corresponding to the monitored wavelengths. The choices for excitation wavelengths to measure emission spectra and emission wavelengths to measure excitation spectra were dependent on the behaviour of the samples. The emission and excitation slits were set to 0.4 mm and 0.8 mm while recording excitation spectra and 1.5 mm and 0.3 mm while recording emission spectra. The increment in both excitation and emission was 0.5 nm. For measurements at low temperature (12 K) the cooling of the sample was achieved under a liquid helium-closed cryostat.

The time resolved emission spectra measurement (12 K) were acquired with the set up used for the steady state PL by changing the excitation source to a 150 W Xe - Hg flash lamp (6μs pulse at half width and 20-30 μs tail). The excitation wavelength was fixed at 370 nm and the emission and excitation slit width were set to 2 mm and 1mm, respectively. In the measurement, an increment of 1nm, a sample window (acquisition time) of 5 ms, an initial delay (time between the end of the pulse and beginning of the measurement) between 0.05 ms and 100 ms, a total flash count of 100, and a total time per flash (depending on initial delay and sample window) between 41ms and 150 ms were used.

In both steady state and TRES, the white light of the excitation sources pass through the excitation monochromator which consists of a grating and set of mirrors to allow dispersion of light into different wavelengths and select the appropriate one. The selected light which passes the excitation monochromator interacts with sample where it gets absorbed. After absorption the excited sample emit photons of different energies. The emitted photons pass through the emission monochromator and get detected. The detected photons are converted to interpretable data and appear as spectrum on the computer.

Absolute Emission Quantum yields:

The absolute emission quantum yields were measured at room temperature using a quantum yield measurement system C9920-02 from Hamamatsu with a 150 W Xenon lamp coupled to a monochromator for wavelength discrimination, an integrating sphere as sample chamber and a multi channel analyzer for signal detection. The method is accurate to within 10%.

Chapter 6: Results and discussions

As indicated in section 5.1, a series of samples was prepared by doping the di-ureasil with either of the rhodamine dyes of different concentrations. Among them we considered the first two samples, with dilute (0.008%) and concentrated (0.1%), both from samples doped with rhodamine B and 6G to discuss the absorption, photoluminescence and x-ray diffraction results. As our discussions are limited to samples with the concentration of the dyes mentioned here, the terms dilute and concentrated are reserved for samples doped with 0.008% and 0.1% concentrations respectively.

6.1 X-ray diffraction results

The room temperature powder diffraction pattern for the di-ureasil hybrids doped with rhodamine 6G and B dyes with concentrations of 0.008% and 0.1% are shown in Figure 17. In both cases, a broad peak centred between 21.0º and 22.0º, a broad weak hump at ~45º, a shoulder between 12º and 14º, and peak at small angle ~2.5º are clearly observed from the diffractograms. The XRD diffraction pattern for the undoped di-ureasil is also included in the graph for comparison purpose (black line in the plots).

The structural features of the di-ureasil under study and other similar hybrid materials have been broadly studied [26, 28, 29, 38]. According to the studies, peaks, shoulder and hump were observed and attributed to different structural features of the di-ureasil hybrid material. The peak observed between 21º and 22º was attributed to the presence of amorphous siliceous domains. The broad weak hump observed between 40º- 45º was identified as the second order peak of the peak indicating the presence of the amorphous siliceous domain whose first order is peaked between 21º and 22º [26, 28, 38]. The shoulder between 12º and 14º was related to intra- siloxane domains in plane ordering [28]. Finally, the peak seen at the lower angle was attributed to the interparticle scattering interference of the siliceous domain in a polymer rich medium [28]. The position of this peak depends on the molecular weight of the polymer and shifts to lower angle monotonically with increase of the polymer molecular weight [39, 40].

Comparing the XRD diffraction patterns of the doped di-ureasil with the undoped one they show the same general behaviours. But, when the di-ureasil is doped with dyes, the peak at small angle is shifted more to the lower angular position as can be seen from the graphs.

This is due to the incorporation of the dye in the polymeric region of the di-ureasil which pushes the siliceous clusters apart.

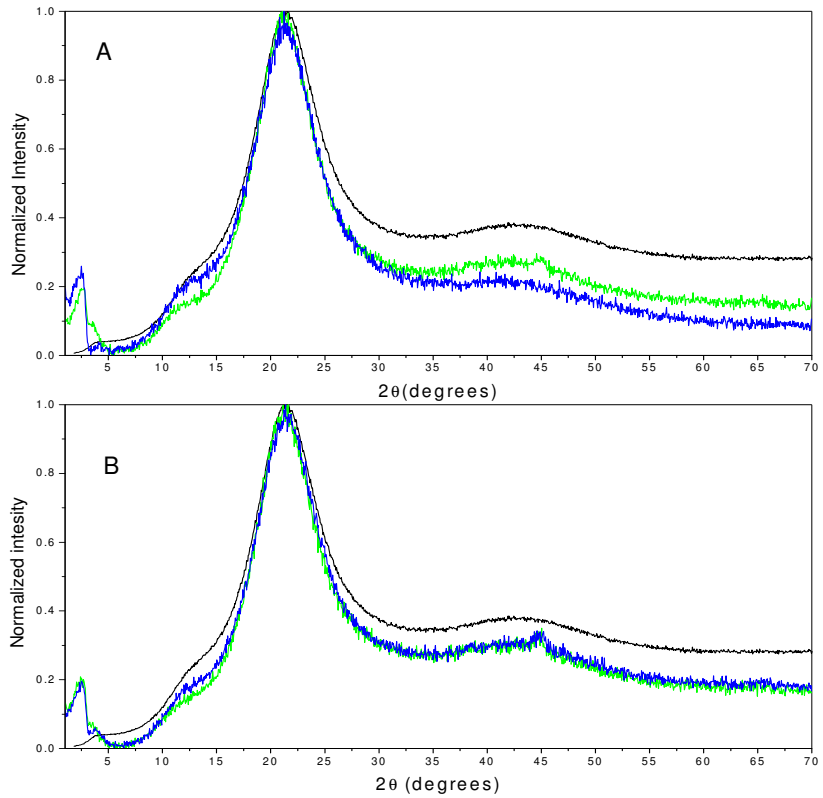

Figure 17: XRD patterns of neat and doped di-ureasil hybrid materials. A) Neat and R6G doped di-ureasils. B) Neat and RB doped di-ureasils. In both cases, the black, green and blue lines stand for the patterns of undoped di-ureasil, di-ureasil doped with 0.008% of RB or R6G, and di-ureasil doped with 0.1% of RB or R6G respectively.

To make the comparisons quantitative, parameters such as the structural unit distance (d), coherent length (L) over which the structural unit survives, characteristic distance related to intra-siloxane domain in-plane ordering (d_p), and average interparticle distance from the maximum peak position of the peak observed due to interparticle scattering (d_s) have been calculated and tabulated in Table 1 for both the doped and un doped di-ureasils.
Bragg's equation (eq. 4.5) was used to calculate d, d_p and d_s. Similarly, the coherent length was calculated by fitting the XRD patterns with pseudo-voigt functions and modified Scherrer equation [28]:

$$L = \frac{I\lambda}{A\cos\theta}, \ldots\ldots\ldots\ldots\ldots (6.1)$$

where, L is coherent length, A, in radians, is the integrated area of peaks and I is its intensity. In addition to the calculated lengths, the angles at which peaks and shoulders of the diffraction patterns observed are included in the table.

Table 1: Calculated interparticle scattering distances, structural unit distances, coherent lengths and the diffraction angles of the XRD data.

Parameters	R6G doped di-ureasil (0.008%)	R6G doped di-ureasil (0.1%)	RB doped di-ureasil (0.008%)	RB doped di-ureasil (0.1%)	undoped di-ureasil
2θ (º) (amorphous siliceous domain)	21.07	21.23	21.63	21.38	21.53
d (Å)	4.21	4.18	4.10	4.15	4.12
L (Å)	10.75	10.44	10.26	10.36	10.32
2θ (º) (2^{nd} order peak position of amorphous siliceous domain)	40 - 45	40-45	40 - 45	40 - 45	40 - 45
2θ (º) (shoulder)	12-14	12-14	12-14	12-14	12-14
d_p (Å)	7.00±0.50	7.00±0.50	7.00±0.50	7.00±0.50	7.00 ± 0.50
2θ (º) small angle peak	2.38 - 2.53	2.38 - 2.53	2.38 - 2.58	2.38 - 2.53	3 - 4
d_s (Å)	35.94±1.00	35.94±1.00	35.58±1.00	35.94±1.00	25.21 ± 2.00

As can be seen from the graphs and the results in the Table, there are no significant differences between the XRD results of the pure di-ureasil hybrid material [28] and the doped ones. The calculated distances and the 2θ position of the peaks are showing the structural characteristic of the neat di-ureasil hybrid material [26, 28]. Therefore, the presence of the-dye in the di-ureasil does not significantly interfere with the structure of the di-ureasil. However, when the dye is doped to the di-ureasil, the small angle peak is shifted by about 0.5º-1.5º in position compared with the diffraction patterns of the undoped di-ureasil (see

Table 1) [28]. As a result, the distance between the siliceous clusters of the di-ureasil increased by about 10Å. This indicates the incorporation of the dye into the organic region of the hybrid material as mentioned above. The incorporation of the dye into the organic domain of the di-ureasil changes the conformation of the polymer chains between the siliceous clusters and eventually increases the distance between them [39, 40]. Yet, the probability that the dye molecules occupy a place in the siliceous domain of the di-ureasil cannot be ruled out. This can be proved from the decrease in the relative intensity of diffraction peaks attributed to the amorphous siliceous domains of the doped di-ureasil as compared to the neat one. Furthermore, for the R6G doped di-ureasil, the decrease in the diffraction intensity is observed with the increase in the concentration of the dye. This supports the argument that the dye may also be incorporated into the inorganic domain of the di-ureasil.

6.2 Absorption spectroscopy

The visible absorption spectra measurements were made in diffuse reflectance mode and are given in Figure 18 for samples doped with both the rhodamine 6G and B dyes. The diffuse reflectance data were converted to the absorbance by using Kubelka-Munk equation [41]. It relates the ratio of absorption coefficient to the scattering coefficient and the reflectance as

$$\frac{K}{S} = \frac{(1-R)^2}{2R}, \quad \text{..... (6.2)}$$

where K and S are absorption and scattering coefficients with dimension of $(\text{distance})^{-1}$ and R represents the reflectance. The plot is therefore given as the variation between the ratio of the two coefficients with respect to wavelength for both rhodamine dyes doped to the di-ureasil hybrid material.

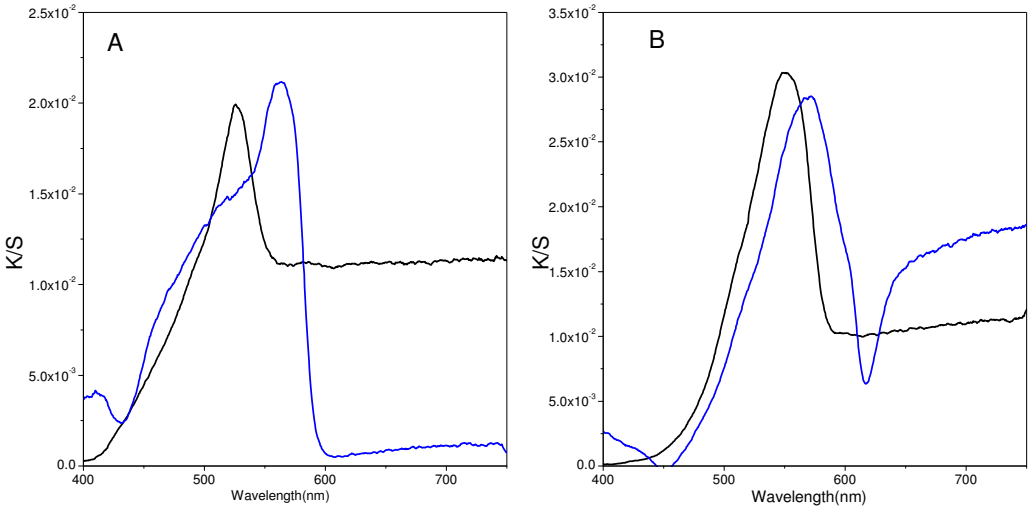

Figure 18: Absorbance (K/S) spectra of the rhodamine dyes doped to di-ureasil hybrid material. A) R6G doped hybrid. B) RB doped hybrid. Black and blue lines show 0.008% and 0.1% concentrations in both cases.

The absorbance spectra of samples doped with rhodamine 6G is shown in Figure 18A. The maximum absorption peak for the sample doped with dilute R6G is shown at 526 nm. However, when the concentration of the dye increases from 0.008% to 0.1% the absorption spectrum shows a shift in peak position to the higher wavelength which is observed at 564 nm and the band is also broader than the dilute R6G doped sample. Similarly, the absorption spectra of the samples doped with rhodamine B, given in Figure 18 B, show maximum absorption peaks at 548 nm and 572 nm for dilute and concentrated samples respectively. In both cases, when the concentration of the dyes increases there are shifts in the peak position of the absorbance and the broadening of the band. These shifts in peak positions of the absorbance and broadening of bands are due to the formation of different types of dye aggregates with the increase in the concentration of the dyes [5, 12].

In general, when the concentration of a light absorbing unit increases, spectroscopic characteristics such as absorbance, emission and excitation spectra of a given material are changed. This is due to different types of associations (aggregates) formed between the light absorbing units. The change in the spectral properties could be splitting of bands and shift in the spectral positions as observed in the absorbance spectra above.

Exciton theory [12, 42], a quantum molecular theory based on the dipole-dipole interactions of monomeric units in the aggregates is a frequently used model to interpret these spectral changes. It predicts different electronic energy diagram and photophysical behaviours of dimers depending on the geometric distribution of the monomer units in the aggregates.

For moderate concentration, the first stage of dye aggregation is the formation of dimers. However, with increasing the concentration further, the aggregation may include trimers, and higher order aggregates as well. According to the model, the expression showing the explicit dependence of the dimers electronic energy level on the geometric parameters is given by

$$\xi(r,\alpha,\theta) = \frac{|M|^2}{r^3}\left(\cos\alpha - 3\cos^2\theta\right) \quad \text{(6. 3)}$$

Here, *M* represents the magnitude of transition dipole moment of the monomer*; r* represents centre to centre distance of the monomers, α represents an angle between transition dipole moment axes of the monomers, θ represents the angle made by transition dipole moment of the unit molecule with the line joining the centres of the monomers, and ξ represents the exciton splitting energy.

With this in mind, let's considering some specific geometrical arrangements that form dimers as shown schematically in Figure 19 and discuss the possible energy levels formed as a result of dimerization and their corresponding spectroscopic effects. In the course of the discussion oval shapes are used to represent molecules and the double arrows in the ovals are used to represent the transition dipole moments as indicated in Figure 19.

Parallel transition dipoles

This arrangement is some times called as perfect sandwich dimers (H-dimers, see arrangement A in figure 19) [12, 42-45]. In this arrangement the transition dipole moments of the monomeric units are aligned in parallel plane resulting in the angle between the dipole moments of the monomeric units, $\alpha = 0^{o}$, and the angle between the dipole moments and the line joining the centres of the monomers, $\theta = 90^{o}$. With this values inserted into equation (6.3), one can determine the exciton splitting energy and thus the energy level of the dimers. As the resultant oscillator strength is 2*f* (assuming *f* as the oscillator strength of

a monomer) for the higher energy state and 0 for the lower one, the allowed spectroscopic transition is only possible from ground state to the higher excited state [12, 42]. Thus, the absorption spectrum of the dimer is observed at higher energy (blue shift) compared with the monomers absorption.

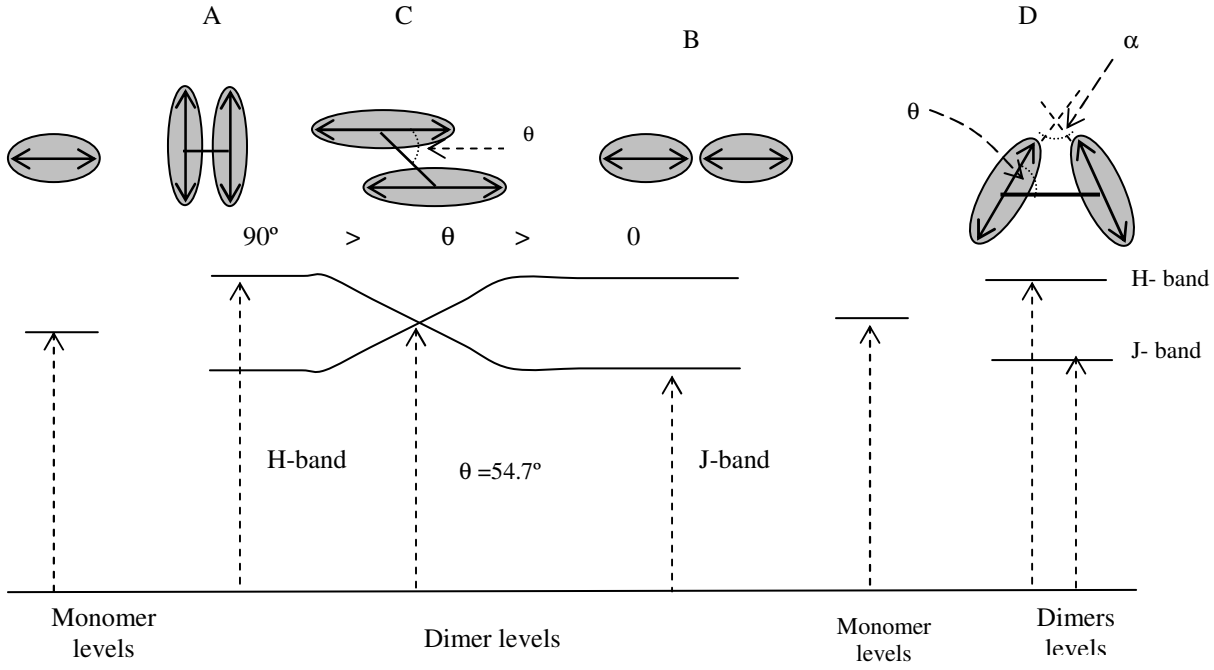

Figure 19: Exciton band energy diagram for molecular dimers.

In line transition dipoles

This is a head to tail arrangement between the monomeric units (see arrangement B in figure 19). Both the angles between the transition dipole moments of the monomers and the angle between the dipole moments and the line connecting the centres of the monomers are 0. In this arrangement the only allowed spectroscopic transition is the transition from the ground state to the lower excited state. This follows from the zero and *2f* resultant oscillator strength in the higher and lower excited states respectively. As a result, the absorption spectrum observed should be shifted to the higher wavelength region compared to the monomer spectrum (red shift). This type of dimer is known as J-dimer.

The parallel and head to tail arrangements of molecules discussed above are ideal cases; because angles (θ and α) of aggregating molecules can take any value. Obviously, the fi-

nal geometry of the dimer is due to the interaction between the dipoles and steric hindrance between monomers in aggregates [12a].

Oblique transition dipoles

In this arrangement, the two angles can assume any value, but satisfy the $\alpha + 2\theta = 180^{\circ}$ condition (see arrangement D in figure 19). The resultant oscillator strength in both of the split excited states are non zero. As a result of this both the transitions from ground state to excited states are possible. The final effect on the absorption band as compared to the monomeric band is band splitting.

Co- planar inclined transition dipoles

In this geometry the angle between the transition dipole moments is 0º while the angle between the transition dipole moments and the line joining the centers can take any value between 0º and 90º (see arrangement C in figure 19). Thus, this arrangement includes both the parallel and in-line transition moment arrangements when the angle θ assumes extreme values. At the angle $\theta = 54.7^{\circ}$ the exciton splitting energy is zero, i.e., the dipole-dipole interactions is zero for this orientation of transition dipole moments of the molecules, irrespective of intermolecular distance [42-45]. Along with this, dimers with $\theta < 54.7^{\circ}$, J-dimers, are know as fluorescent while dimers with $\theta > 54.7^{\circ}$, H-dimers, are non fluorescent dimers [12, 42].

Employing this discussion to our case, the shift in the absorbance peak positions of samples doped with either of the rhodamine dyes with the increase in concentration is due to the formation of the dimers and higher order aggregates [46]. As the shift observed with the increase in concentration is to the higher wavelength regions, the dimers formed are the J-dimers even though other possibilities can not be ignored. Further spectroscopic analyses of the aggregate formation of the dyes follow under the topic of PL spectroscopy in the next section.

6.3 Photoluminescence spectroscopy

In this section, the photoluminescence results for di-ureasil hybrid material doped with rhodamine 6G and B are presented and discussed.

6.3.1 Rhodamine B doped hybrid materials

6.3.1.1 Emission spectra of dilute rhodamine B doped hybrid material

Figure 20 A and B show the emission spectra of the dilute rhodamine B doped di-ureasil hybrid material acquired at 12 K and 300 K respectively. The spectra are taken by exciting the sample with different excitation wavelengths as shown in Figure 20. Moreover, the spectra are height normalized to ease the visualization.

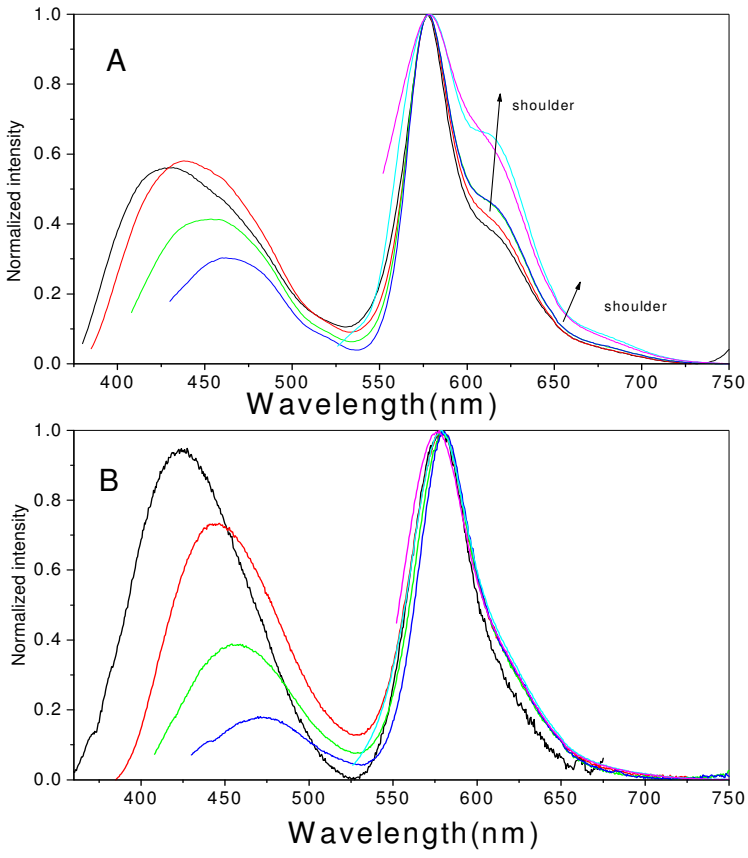

Figure 20: Emission spectra of the di-ureasil hybrid material doped with dilute RB acquired at A) 12 K. B) 300 K. The black, red, green, blue, cyan, and magenta lines show excitation wavelengths of 345 nm, 370 nm, 393 nm, 415 nm, 511 nm, and 537 nm respectively.

The emission spectra for both temperatures show that there are two emission bands which are clearly observed in the ranges between 360-530 nm and 530-700 nm.

The band observed in a high energy range shows a broad emission band emitting from the purplish-blue–green. The origin of the emission in this range comes from the di-ureasil hybrid material [26, 28, 47]. These emission spectra are characterized by the presence of bands arising from the processes occurring in both inorganic and organic domains of the di-ureasil hybrid. Radiative recombination occurring within the nanometric sized siliceous domain associated with oxygen related defects [47] ensures the presence of the purplish-blue band. On the other hand, the emission arising from the urea bridge, NH, gives the relatively broad blue-green band [26, 32, 39, 47].

The emission peak positions of the host material are seen to shift to the lower energy value with increasing excitation wavelength from 345-415 nm. This is a typical characteristic feature of the urea cross linked hybrid material. The reason why this shift occurred with the increase in the excitation wavelength can be argued using a concept called 'thermalization gap' (E_0) [26, 31]. This is an energy which gives demarcation to whether there is an energy shift or not. As such, if charge carriers (electrons or holes) are exited with excitation energy greater than the 'thermalization gap' then they relax to the same energy level before recombination. Thus, there is no shift in the peak position of the emission spectra. However, when the exciting photon is below this energy value (i.e. the excitation wavelength increases), the carriers are excited to the electronic states with energy below E_0. These states are known as localized band tail states. Thus, carriers excited to these states recombine radiatively and the emitted photon will be a low energy photon, which ultimately shows the red shift in peaks.

The emission band which appeared to the lower energy range (1.77 eV- 2.34 eV) is originated from guest molecules, rhodamine B dyes. The peaks of these bands (for different excitation wavelengths) do not significantly shift with the excitation wavelengths and their maximum is centred around 577 nm. Besides this, the emission band observed here does not show a Gaussian profile. This signifies that there are more than one emitting components with different fluorescence efficiency contributing to the observed emission band. The presence of these emitting components can be seen from the shoulders which appeared in the wavelength ranges of 600-625 nm and 630-675 nm in the emission bands of the spectra taken at room temperature (Figure 20 B). These shoulders are clearly observed in

the emission band acquired at low temperature (12 K), which grow to a relatively observable band (Figure 20 A). To quantify the energy of these emitting components, a fitting was performed on the emission spectrum which was recorded by exciting the sample at 511 nm (2.43 eV) (see Figure 21). The selection of this spectrum is due to the fact that the emission band from the host does not appear as a result of the emission monochromator scanning the range of wavelength where the emission from host does not exist.

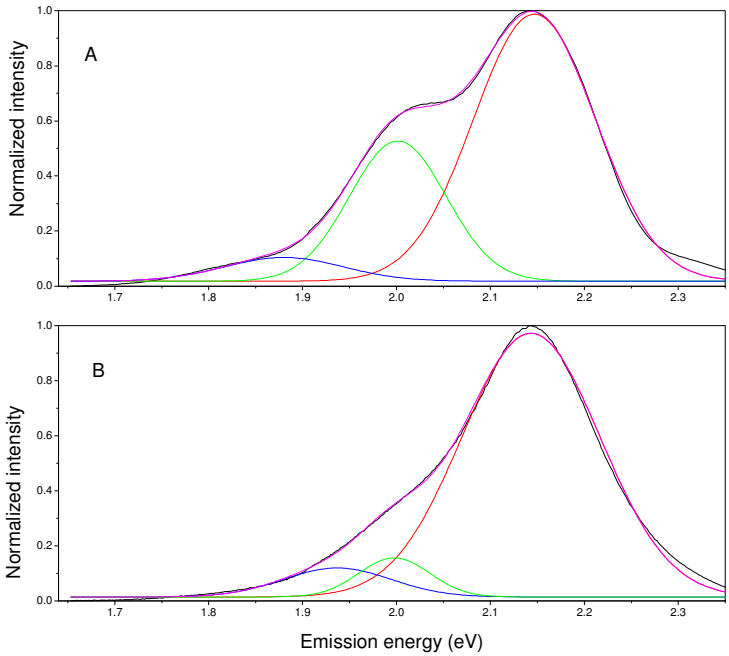

Figure 21: Curve fitting on emission spectra of di-ureasil doped with dilute RB dye excited at 511 nm. A) Emission at 12 K. B) Emission at 300 K. In both cases, the black lines stand for original emission, red, green, and blue lines stand for Gaussian fittings and magenta stands for the envelop.

The fit was performed on both the spectrum at low and room temperatures. First, the spectrum at low temperature was fitted to three Gaussian curves by selecting the main peak and peaks of the clearly observed shoulders (Figure 21A). Then, the same peak positions fixed for spectrum at low temperature were used to fit the spectrum at room temperature to three Gaussian curves (Figure 21 B). The existence of more than one emitting components can be attributed to the presence of different types of aggregates formed at different geometries as discussed in the absorbance result [12b].

Comparing the intensities of the spectra with respect to measurement temperatures, the spectra measured at low temperature are very intense than the spectra acquired at room

temperature. Figure 22 shows the spectra of the dilute rhodamine B doped hybrid material by exciting the sample at different wavelengths for 12 K and 300 K temperature values. As can be seen from the figure, for each exciting wavelength used, the intensity of the spectrum measured at low temperature is higher than the intesnity of the spectrum mesured at room temperature.

This difference in intensity due to the temperature is from the fact that the temperature of the system is the root cause for molecular vibration. At high temperature, molecules can tumble around randomly. With the temperature of the system decreasing the random molecular motion, and collision decreases but the molecule never be at rest. This process has siginificant effect on the emission intensity of a material. When the temperature of the system increses, the random motion of molecules increase and nonradiative de-activation mechanisms such as vibrational relaxation, internal conversion, and intersystem crossing will be highly competitive. Thus, the intensity of emitted radiation is low. However, when the temperature of the system decreases, the fluorescence is more dominant over the other non radiative de-activation processes and the intensity becomes higher.

The other intersting effect observed here is that for either of the temperatures, the relative intensity of the emission from rhodamine dye increases with increasing the excitation wavelengths from 345 nm to 511 nm. This is related to the fact that the more a molecule absorbs the more the emission will be. In this case, the wavelengths from 345-415 nm are selected from the excitation band of the hybrid material (see Figure 24 below). Thus, the emission of the dye is due to the energy transfer from the host to the dye. However, the 511 nm wavelength selceted from the absorption region of the dye and this leads to higher emission intensity than the other wavelengths.

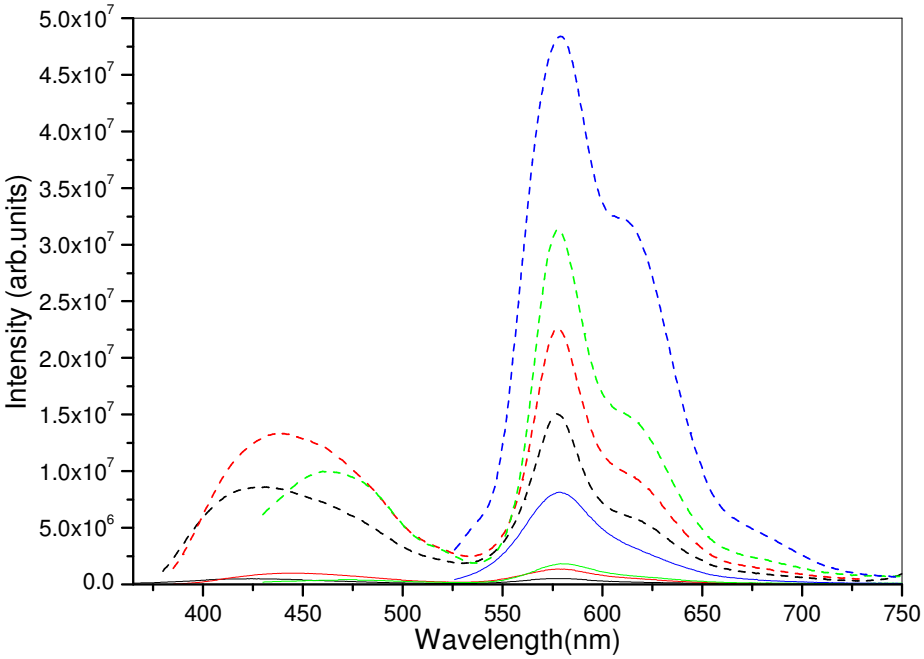

Figure 22: Emission spectra of dilute RB doped sample for different excitation wavelengths: The black, red, green and blue lines stand for emission at excitation wavelengths of 345 nm, 370 nm, 415 nm, and 511 nm and the solid and broken lines stand for emission at 300 K and 12 K respectively.

6.3.1.2 Time resolved emission spectra (TRES) of a dilute RB doped di-ureasil hybrid material

The time resolved emission spectra at low temperature (12 K) for the dilute rhodamine B doped sample at different delay times (0.05 ms-100 ms) and sample window of 5.0 ms is shown in Figure 23. For the emission band from the host, there is a decrease in the intensity of the peak at the lower wavelength region (around 425 nm) with the increase in the initial delay time. However, the emission at the higher wavelength region centred around 500 nm exists even after longer initial delay times. The TRES for the host emission region show the co-existence of the purplish-blue and blue-green bands and the fact that the recombination processes of holes and electrons responsible for the respective emission bands of the di-ureasil happen at different life times [26]. The fast decrease of the intensity at 425 nm with the increase in delay times shows that the siliceous emitting centers are short living components. Similarly, the band shown on the higher wavelength region is the TRES of the dye emission band. With the delay time increasing the shape of the spectrum is preserved (see the inset in the figure), showing that the emitting centers for the main band and

shoulders have lifetimes comparable with the longer wavelength (500 nm) emitting center of the di-ureasil hybrid material.

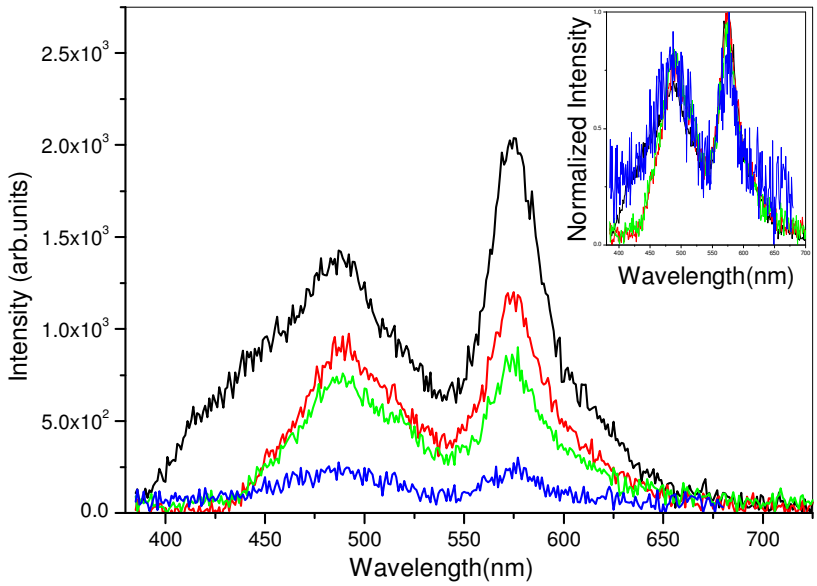

Figure 23: Time resolved emission spectra for the dilute RB doped sample excited at 370 nm for a sample window of 5.0 ms at 12 K. The black, red, green and blue lines show delay times of 0.05 ms, 5.0 ms, 20 ms, and 100 ms respectively.

6.3.1.3 Excitation spectra of dilute rhodamine B doped hybrid material

The excitation spectra of the dilute rhodamine B doped sample acquired at 12 K and 300 K temperatures are shown in Figure 24 A and B respectively. The spectra were taken by monitoring the emission wavelengths selected from the two respective emission bands; the dye and host emission bands. As such, one can see the excitation spectra by dividing into two categories: excitation spectra whose monitored wavelengths are from the host emission band and dye emission band. The spectra acquired by monitoring the emission wavelengths from the host emission band (410-475 nm for low temperature (Figure 24 A) and 410-440 nm for room temperature (Figure 24 B)) are shown in the lower wavelength region.

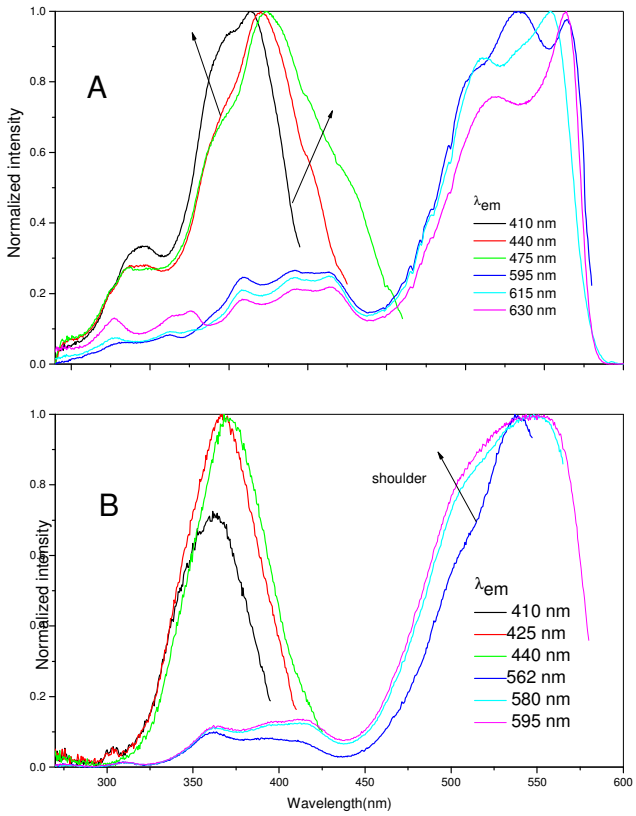

Figure 24: Excitation spectra of di-ureasil doped with dilute RB for different monitored emission wavelengths (λ_{em}). A) at 12 K. B) at 300 K. The arrows are indicating shoulders.

The spectra recorded at room temperature by monitoring the emission wavelengths at 410, 425, and 440 nm show a large broad band between 280 and 425 nm. Two peaks centred around 300 nm and between 360 nm and 375 nm are clearly seen. When the monitored wavelength increases, the peak positions between 360 and 375 nm are red shifted. Moreover, with the increase in monitored wavelength the broadening of the excitation band is also observed. As such, the full width at half maximum (fwhm) show increment from 51.66 nm to 53.95 nm when the excitation wavelength increases from 410 to 440 nm. The red shift in the peaks and broadening of the band are characteristics of the di-ureasil hybrid materials [26, 30, 47, 48].

When the temperature decreases from 300 K to 12 K, the peak at 300 nm is observed relatively intense and does not shift with the increase in the monitored emission wavelengths. The main excitation band peaked between 360 and 375 nm is shown to be broader than the

one at the room temperature and the peak position shift with the increase in the monitored emission wavelength. Moreover, there are shoulders (indicated by arrows) observed both to the left and right sides of the principal excitation peaks. This can be clearly seen by comparing the excitation spectra of the low and room temperatures monitored at the same wavelength (Figure 25 A). Since the monitored wavelengths are selected from the purplish-blue emission band of the di-ureasil, in both cases, the observed excitation peak in between 360 nm and 375 nm is exactly in the energy range which is attributed to excite the inorganic domain of the di-ureasil [26, 32].

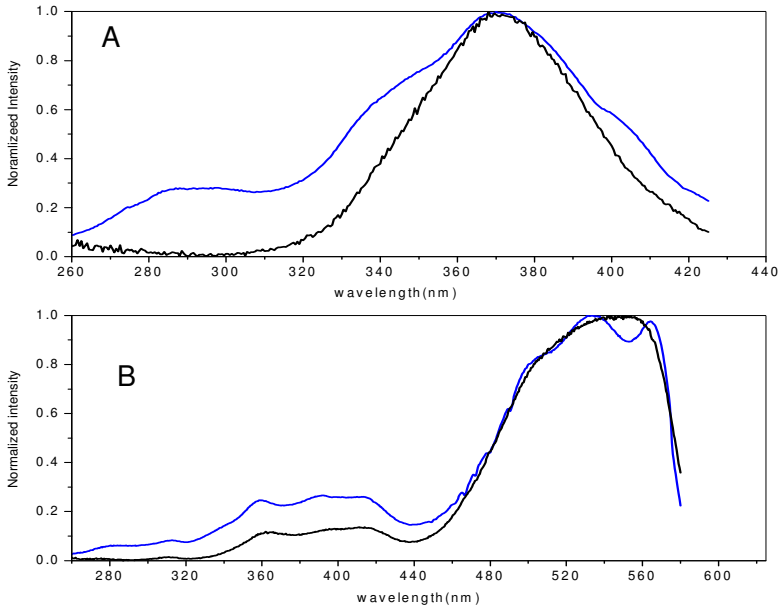

Figure 25: Excitation spectra of di-ureasil doped with dilute RB monitored at emission wavelength A) 440 nm and B) 595 nm. The blue and black lines show the spectra at 12 K and 300 K respectively.

The excitation spectra by monitoring the emission wavelength from the emission band of the dye (595-630 nm for low temperature (Figure 24 A) and 562-595 nm for room temperature (Figure 24 B)) are shown by the spectra extending from the lower to the higher wavelength regions. They show typical excitation spectra of rhodamine B, which looks like absorption spectra of rhodamine B in an ethanol solution [49].

As can be seen from the spectra, there is a broad band observed in the lower wavelength regions (in the excitation bands of the host). This is a region in which the dye does not absorb much. Thus, the appearance of the broad band in this range indicates the presence of transfer of energy from the host to the dye molecules.

The visible region (for wavelength greater than 400 nm) excitation spectra at room temperature show broad band with shoulders shown around 504 nm and main peaks ranging between 537-548 nm as monitored wavelength increase from 562 to 595 nm (Figure 24 B). In addition to this, the shoulders become intense and the spectra become broader with the monitored wavelength increasing. This shift of the excitation peak with the increase in monitored wavelength might be due to the large number of dimers whose electronic energy levels lie within the lower energy values. These kind of dimers are known as J-dimers and they are characterized by absorbing low energy photons when compared to pure monomers as discussed in section 6.2 [5, 12a, 42]. Indeed the excitation spectra reveal only the presence of J-dimers as the excitation spectra of the non-fluorescent dimers are zero.
On the other hand, when the temperature decreases to the low temperature value, 12 K, the broad band observed in the room temperature is split into two peaks with the clearly observed shoulders. An apparent difference in the excitation spectra at low and room temperatures for a detection wavelength monitored from the emission band of the dye, 595 nm, is shown in Figure 24 B. As can be seen from Figure 24 B, the spectrum taken at room temperature is peaked at 543.5 nm while the spectrum taken at low temperature has two peaks centred around 533.5 nm and 566 nm. This split of the band at low temperature is an indication of the formation of fluorescent dimers adopting an oblique configuration [42, 44, 50-52] as described in the schematic representation (scheme D) of Figure 19.

6.3.1.4 Emission spectra of concentrated rhodamine B doped hybrid material

The emission spectra for a concentrated rhodamine B doped sample acquired at room temperature are shown in Figure 26. As in the dilute sample, different excitation wavelengths were used to excite the sample and the vertical axis was normalized to easily compare the peaks.

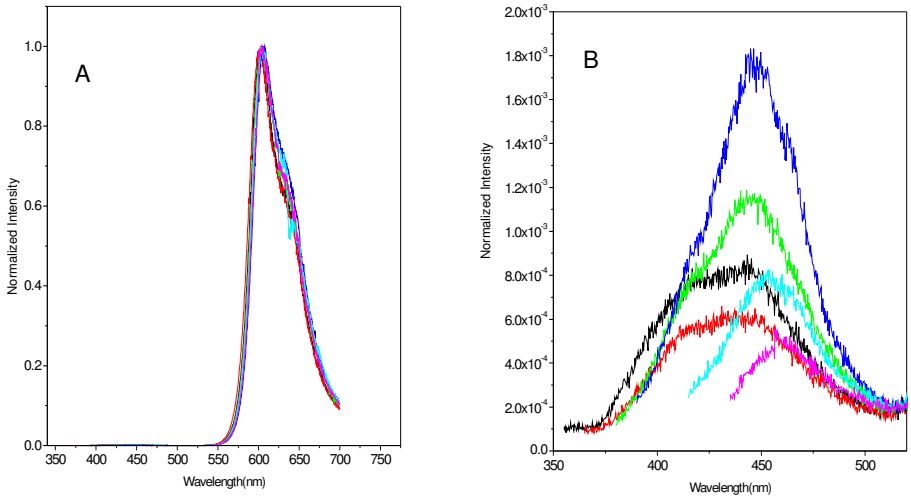

Figure 26: Emission spectra of di-ureasil doped with concentrated RB dye. A) Emission.
B) Amplified emission from the suppressed emission of the host by plotting the data between 350-520 nm. The black, red, green, blue, cyan, and magenta lines show excitation wavelengths of 340 nm, 350 nm, 365 nm, 375 nm, 400 nm, and 420 nm respectively.

With the increase in the concentration of dye from 0.008% to 0.1%, there is a dramatic change observed on the emission spectra of the material as shown in Figure 26 A. The emission band from the di-ureasil hybrid, which was observed in the lower wavelength region for less concentrated sample, is severely suppressed. However, an emission band of very low intensity is still present. Amplifying (by plotting the emission data over a lower wavelength region) the emission in this region verifies the presence of bands whose maxima lie between 440 nm and 460 nm with red shift while increasing the excitation wavelength (see Figure 26 B). This band corresponds to the purplish-blue emission band whose origin is from the recombination process within the nanometeric sized inorganic (siliceous) domain of the di-ureasil hybrid material. Nevertheless, the emission from the or-

ganic bridge, blue-green emission band, is highly suppressed with the increase in concentration of an organic dye.

This disappearance of emission band of the host from where it would have excited was previously reported for another dye doped in a similar host [53]. According to the report, safranine-O dye was doped to a polysilsesquioxane host which contains urea cross linking groups. The difference between this host and the one in the current study is only the use of BSA (4, 4´-[1, 3 phenylenebis-(1-methylethylidene)] bis (aniline)) instead of Jeffamine polymer. And it has clearly shown that doping the di-ureasil hybrid with safranine-O dye suppresses the emission band from the host material, except the one from the purplish-blue region.

This severe decease in the emission intensity from the host has been attributed to the energy transfer from the host to the dye. The important process involved in the energy transfer mechanism is that there is a radiative energy transfer, where one of the two components in interaction with each other, donor (host), absorbs energy and transfers to the second one, accepter (dye molecule), partially or totally. Therefore, the energy transfer from the donor to the accepter exhibits a reduction in the emission of the donor in the excited state and facilitates the emission of the accepter in the excited state [36, 54].

In general, the absorption and energy transfer process follows the following reaction type scheme:

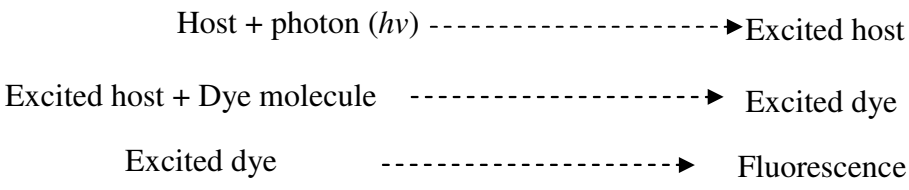

The presence of the energy transfer between the host and dye can be shown by an overlap of the emission band of the host and the excitation band of the dye [36]. Figure 27 shows the plot of the excitation and emission spectra of the dilute rhodamine B doped sample. The overlap of these two spectra signifies the presence of the energy transfer when the concentration of the dye is even less as pointed out above.

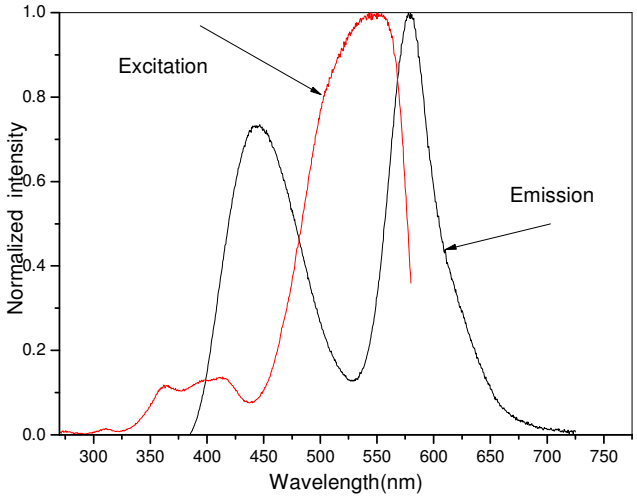

Figure 27: Emission and excitation spectra of sample doped with dilute RB dye. Emission was acquired by exciting wavelength of 370 nm, and excitation spectrum was taken by monitoring the emission at 595 nm.

As mentioned above another indication for the energy transfer can be the decrease in the emission intensity of the donor (di-ureasil hybrid). In this case, when concentration of the doped dye increases the relative emission intensity from the host decreases (see Figure 26 A). This means that with the increase in the concentration of the dye, the emitting centres of the hybrid material find the dye molecules very near to them and make the energy transfer easily. This is due to the fact that the more the accepter moieties are closer to the donor, the easier the energy transfer will be. Similarly, R.S. Ferreira et al. [55] has shown that the dependence of the energy transfer efficiency of the di-ureasil hybrids containing 16 and 40 oxyethylene repeat units on the concentration of dopant; namely the Nd^{3+} ion. Here, it was concluded that when the concentration of the lanthanide ion increases, there are high number of ions located near to the hybrid emitting centres and thus increases the energy transfer probability.

The important point we need to stress here is the highly suppressed blue-green emission band of the host material as compared to the purplish-blue region (Figure 26 B). This shows that the blue-green emitting centres, the organic domains, strongly transferred their energy to the dye molecules [53]. This is favoured if the dye molecules are more concentrated near the organic domains than the siliceous domains. Therefore, we can unequivocally conclude that the organic domains are the favourable sites for the rhodamine B dyes.

This result corroborates the conclusion drawn from the XRD data, indicating that the dye molecules are highly incorporated in the organic domain of the di-ureasil.
The emission bands observed here (in the higher wavelength range) are therefore, the one from the dye. There is no significant shift in peak position with the excitation wavelengths chosen to excite the sample. The shoulders observed in the spectra of the sample with low concentrated dye are clearly observable in this case. This gives clear idea that there are more aggregates of the dyes formed with the increase in concentration as expected. As recognized in the above discussions, these aggregates create different emitting centres which contribute to the observed emission band and the shoulders as well [12, 43].

6.3.2 Rhodamine 6G doped hybrid materials

6.3.2.1 Emission spectra of dilute rhodamine 6G doped hybrid material

The emission spectra of the dilute rhodamine 6G dye doped with di-ureasil hybrid material are shown in Figure 28A. The vertical axis is normalized to make the comparison of the peak positions easy. The emission spectra were acquired by exciting the sample with different excitation wavelengths ranging from 350 nm to 524 nm (Figure 28A).

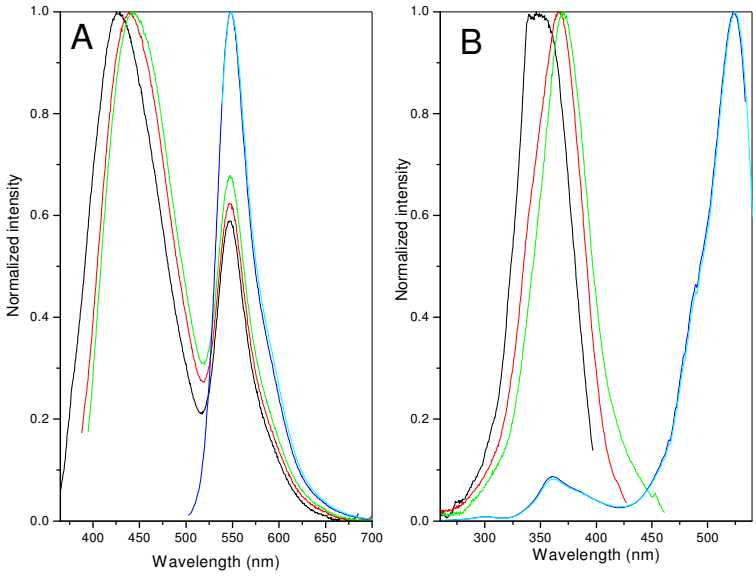

Figure 28: Emission and excitation spectra of dilute R6G doped di-ureasil hybrid material at 300 K. A) Emission: the black, red, green, blue and cyan lines indicate excitation wavelengths of 350 nm, 367 nm, 380 nm, 488 nm, and 524 nm respectively. B) Excitation: the black, red, green, blue and cyan lines indicate monitored emission wavelengths of 412 nm, 442 nm, 476 nm, 549 nm, and 565 nm respectively.

As seen in the spectra (Figure 28A), there are two emission bands observed in the wavelength ranges between 365-500nm and 500-675nm respectively. Like the spectra for dilute RB dye doped material discussed above, the former band which is shown in the higher energy range corresponds to the emission from the processes within the di-ureasil (host) [26, 28, 32, 47, 56]. With the increase in the excitation wavelength from 350-380 nm, a shift in the peak position of the emission from 429-443 nm was observed. As for the samples doped with rhodamine B, this high dependence of the emission peak position on the excitation wavelength is the characteristic feature of the di-ureasil hybrid materials [26].
The spectra observed in the lower energy range are originated from the rhodamine 6G dye molecules. The peak positions of these spectra are centred around 548 nm and do not show a significant shift with the excitation wavelength increasing as opposed to the host emission. But, compared to the emission spectra of rhodamine 6G in an ethanol solution (556 nm) [49], the peak position of the rhodamine 6G in the di-ureasil hybrid is shifted to the lower wavelength region by about 8 nm. In the same argument with red shift in the fluorescence of dilute RB doped sample, the blue-shift in the fluorescence peak position of the sample doped with dilute rhodamine 6G compared to its fluorescence in ethanol is due to a different physicochemical environments that the di-ureasil provides the dye as compared to the ethanol [12b]. The spectra however, do not show Gaussian emission bands. These indicates the presence of more than one emitting components which arise from different types of possible aggregations that the dye molecules form with each other [42].

6.3.2.2 Excitation spectra of dilute rhodamine 6G doped hybrid material

The excitation spectra for dilute rhodamine 6G doped sample monitored at different emission wavelengths (412 nm - 565 nm) are shown in Figure **28**B. Similar to the rhodamine B doped samples, the monitored wavelengths were chosen both from the host (412 nm - 476 nm) and dye (534 nm -565 nm) emission bands.
For the monitored wavelengths selected from host emission band, the excitation spectra show a large broad band between 280 nm - 455 nm. With the monitored energy decreasing, red shift in the peak position (340 nm - 348 nm) and widening of the spectra were observed. The red shift in the peak position of the excitation spectra is the unique feature of the di-ureasil hybrid materials [26, 28]. The band widening observed here was reported previously by Fu et al. [24] and attributed to the existence of more than one absorbing

components; the NH group and the siliceous domain. These components were also observed by the excitation spectra at low temperature (14 K) for the undoped di-ureasil [26, 32]. The NH absorbing unit was assigned to the preferential excitation of the broad blue-green emission band whereas the purple-blue emission band arises from the recombination process within the siliceous domain [32].

The excitation spectra recorded by monitoring the wavelength from the emission band of the dye are also shown in Figure 28 B by the curves extending from lower wavelength regions to the higher wavelength regions. Two bands, peaked at 360 nm and 524 nm, and shoulder at 495 nm were observed. The appearance of the two peaks and shoulder show that the excitation spectra are similar with excitation spectrum of rhodamine 6G dye in ethanol solution [8]. Moreover, the band observed at 360 nm peak signifies the presence of an energy transfer from the host to the rhodamine dye.

6.3.2.3 Emission spectra of concentrated rhodamine 6G doped hybrid materials

The emission spectra of concentrated rhodamine 6G doped hybrid material recorded at room temperature (300 K) are shown in Figure 29 A. Like the emission of the concentrated rhodamine B doped sample, with increasing the concentration of the rhodamine 6G from 0.008% to 0.1% the emission from the host was suppressed from where it would have existed. However, amplifying the band in the low wavelength range (see Figure 29 B) shows the presence of emission from the host with its characteristic red shift property while increasing the excitation wavelength.

With similar argument given for the concentrated rhodamine B doped material, the disappearance of the emission from the host is attributed to the presence of the energy transfer from the hybrid to the dye. Moreover, the complete suppression of the blue-green emission band whose origin is the organic domain of the di-ureasil shows that there is a stronger transfer of energy from the organic domain of the di-ureasil than the one from siliceous domain. This may indicate that the rhodamine 6G dye is preferably closer to the organic domain than the siliceous domain of the di-ureasil hybrid.

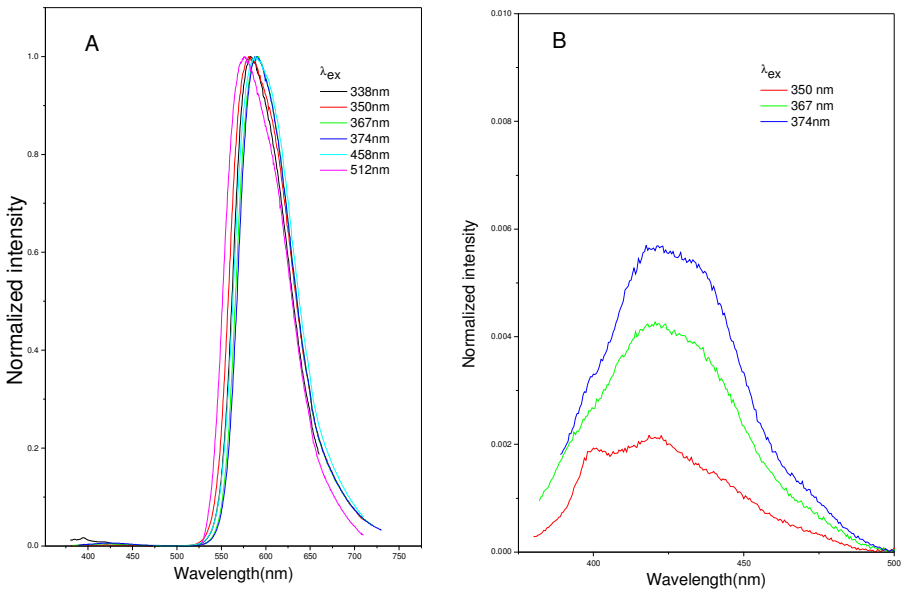

Figure 29: Emission spectra of concentrated R6G doped di-ureasil hybrid material at different excitation wavelengths (λ_{ex}). A) Emission. B) Amplified emission from the suppressed band of the di-ureasil emission region plotted from 350 nm-500 nm.

The spectra observed at the higher wavelength range are therefore, the emission spectra whose origin is the rhodamine 6G dye. Due to the increase in concentration of the dye, the peaks are shifted to the higher wavelength region. As a result of this, the peak positions of the spectra are observed at wavelengths greater than ~575 nm. This shift in position from position of the less concentrated dye is because of the formation of J-dimers with the increase of concentration as shown in Figure 19 B [12b].

6.3.3 Comparison of the two rhodamine dyes doped hybrid materials

In this section comparisons of the effects of both dyes, rhodamine 6G and B, doped into di-ureasil hybrid material will be considered and discussed. To simplify the comparison we considered the emission spectra at excitation wavelength of 350 nm, excitation spectra whose monitored wavelength is from the di-ureasil emission band at 440 nm, and the excitation spectra by monitoring the emission wavelength from the dye emission band at 595 nm for dilute and concentrated samples doped with both dyes.

Figure 30 shows the emission spectra of both rhodamine B and 6G doped samples by exciting all the samples at excitation wavelength of 350 nm. For both dyes at lower concen-

tration the emission bands from the host and dye are observed (see black and green lines). This is because both the di-ureasil and the dye are optically active materials and they emit in their respective emission energy ranges [53].

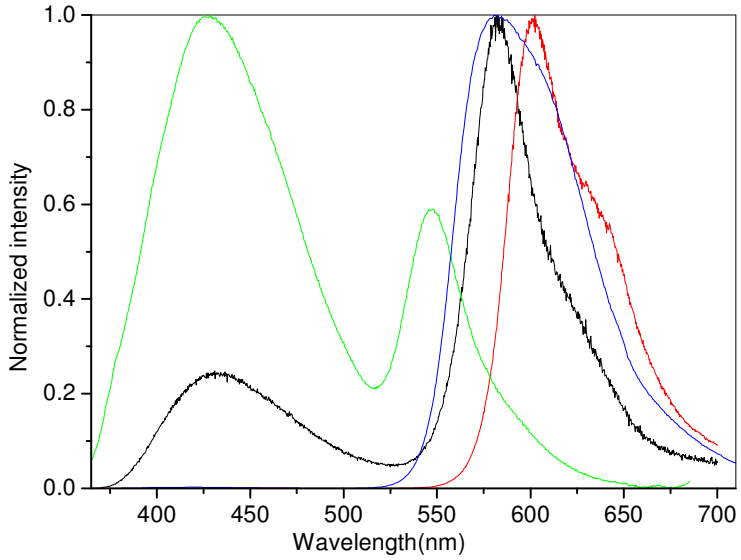

Figure 30: Emission spectra of dilute and concentrated RB and R6G doped di-ureasil hybrid material excited at 350 nm at 300 K. Black (0.008% RB), red (0.1% RB), green (0.008% R6G), and blue (0.1% R6G).

Nevertheless, when the concentration of either of the dyes increases from 0.008% to 0.1%, the band to be appeared from the host does not exist as a result of energy transfer from the host to dye. Comparing the emission of the samples doped with RB and R6G; the peak position of the RB doped sample is shown at higher wavelength in the dye emission band for both concentrations. This is due to the structural difference of the two dyes which depend on the substituents that are attached to the main xanthene structure [3, 8].

For dilute samples, the relative emission intensity of the R6G doped sample is higher than the RB doped one in the di-ureasil emission band (see Figure 30). On the other hand, in the dye emission band, the relative intensity of the RB doped sample is higher than the R6G doped one. When the concentration of both dyes increases the host emission is suppressed as discussed before and the emission intensity from the hybrids material doped with rhodamine 6G dye is higher. This very clear difference manifests itself in the absolute emission quantum yield as well.

Absolute Emission Quantum Yield

Table 2 shows the room temperature absolute emission quantum yield of the neat and doped di-ureasils measured at 375 nm and 380 nm excitation wavelengths respectively. Within the experimental error, the measured absolute emission quantum yield for the neat di-ureasil is the same as the previously reported value [30, 32, 47]. When the di-ureasil hybrid material is doped with rhodamine dyes the absolute emission quantum yield increases.

Table 2: Absolute emission quantum yields of neat, RB and R6G doped di-ureasil hybrid material at excitation wavelengths of 375nm and 380 nm as indicated in the parenthesis.

Samples	Concentration (%)	Emission quantum yields (%)
Undoped di-ureasil (375 nm)	0.0	5
RB doped di-ureasil hybrid (380 nm)	0.008	11
	0.1	65
R6G doped di-ureasil hybrid (380 nm)	0.008	7
	0.1	70

By increasing the concentration of the dyes from 0.008% to 0.1%, the quantum yield of the material increased dramatically. As such, the quantum yield of the di-ureasil doped with RB was increased by a factor of 6 while the quantum yield of the di-ureasil doped with R6G was increased by a factor of 10 (see Table 2) compared to their dilute counterparts. For dilute concentration, the emission quantum yield of the di-ureasil hybrid doped with RB dye is higher than the one doped with R6G dye. However, for the higher concentration, the reverse effect is observed. This is inline with the intensity differences above, showing the intensity of the RB doped material higher than the R6G doped one for dilute concentration and the reveres effect for the higher concentration.

As can be seen from the table, the absolute emission quantum yield of the di-ureasil hybrid material is highly dependent on the concentration of the dopants. The measured values, 65% for RB and 70% for R6G doped di-ureasil hybrid are high enough to realize solid materials for application in light emitting devices, such as laser dyes.

On the other hand, the intensity which was suppressed from the host emission band with the increase in concentration of dyes is relatively higher than the dye emission bands when

the concentration is dilute. Even though, the main reason for this difference in intensity lies on the concentration of the dyes the fact that the excitation wavelength, 350 nm, is chosen from the region where the di-ureasil absorbs more can not be ruled out. The observed intensity of the dye is mostly from the energy which is transferred to it from the host.
As explained above, the suppression of the emission from the host emission region when the concentration of either of the dye increases is due to the definitive energy transfer from the host to the dye [53].
The table given below shows the ratios of integrated intensities for the spectra measured by exciting the samples at 350 nm wavelength. In the table, the ratios of the integrated intensities of the dye emission band to the host emission band $\left(A_{dye} / A_{host} \right)$ for all the samples at different concentrations were considered. The notations used here are: A_{dye} is the integrated intensity of dye emission, A_{host} is integrated intensity of the host emission.

Table 3: Integrated intensity ratios

Samples	R6G (0.008%)	R6G (0.1%)	RB (0.008%)	RB (0.1%)
$\left(A_{dye} / A_{host} \right)$	0.34	448.12	0.68	616.12

As can be seen from Table 3, the ratios of the integrated intensities of the two emission bands of the samples doped with respective dyes show that the ratios calculated for the concentrated samples are very large. This indicates that the transfer of energy is so strong when the concentration increases. For both concentrations, the ratio calculated for samples doped with R6G is less than the ratio calculated for the corresponding samples doped with RB. Assuming the host emission to be the same irrespective of the type of dopants, the higher ratio calculated for RB indicates that it is highly accepting the energy from the host than R6G does.
Another substantial effect observed with the increasing of concentration of either of the rhodamine dyes is the shift in the peak positions of the dye emission bands as compared to their respective dilute sample counterparts. This red shifting of peak is due to the presence of aggregates of the dye molecules [12]. In addition, the shoulders are clearly observed with the increase in concentrations. The reason why the shoulders appeared intense is due

to the formation of large number of aggregates contributing to the emission of these shoulders [12].

Comparing the energy difference between emission maxima of the dilute and concentrated samples, the shift observed for R6G doped samples is higher than the one doped with RB. Taking the difference between the peak positions of the respective spectra (between dilute and concentrated samples), shifts of 34 nm (1051 cm^{-1}) for R6G and 20 nm (564 cm^{-1}) for RB doped samples were calculated respectively. This might show that aggregations formed by the rhodamine 6G dyes are more strongly interacting than those formed by rhodamine B dyes.

The excitation spectra taken by monitoring the emission wavelength from the emission band of dye for the R6G doped sample (Figure 31B) is supportive of the absorbance spectrum which indicates the formation of aggregates of the dye molecules. Comparing the excitation spectra of samples with dilute and higher concentration, one can see that the peak position shifts to higher wavelength region and the intensity of the shoulder also increases with the increase of concentration. This clearly shows the presence of fluorescent aggregate of dyes in the sample [12b].

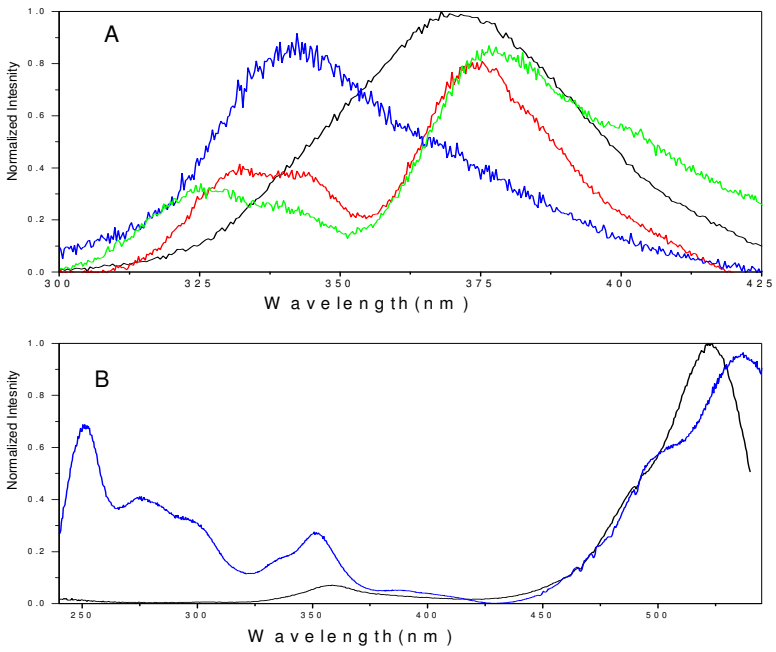

Figure 31: A) Excitation spectra of di-ureasil doped with RB and R6G at 440 nm. Black (0.008% RB), red (0.1% RB), blue (0.008% R6G), and green (0.1% R6G). B) Excitation spectra of di-ureasil doped with R6G at 550 nm. Black (0.008% R6G) and blue (0.1% R6G).

The excitation spectra monitored at the emission wavelengths selected from the emission bands of the host for both dyes are shown in Figure 31A. The excitation spectra of samples doped with dilute concentration of both dyes show large broad bands with shoulders observed in both cases. These are typical profiles of the excitation spectra of neat di-ureasil hybrid material [26, 28]. However, unlike the excitation spectra for neat di-ureasil [26], the absence of the peak showing the urea bridge of the di-ureasil emitting center is related to the energy transfer process. As mentioned above the transfer of energy from the organic domain of the di-ureasil is higher than the one from the inorganic domain. The excitation peak of the R6G doped sample is shown at 340 nm while the RB doped sample is peaked at 368 nm. Both the peaks correspond to the energy range which excites the siliceous domain of neat di-ureasil hybrid material [26]. Nonetheless, the appearance of the excitation peak of the sample doped with RB at a higher wavelength compared to the R6G doped sample indicates that the emission of the di-ureasil doped with RB has more contribution from the organic domain of the di-ureasil.

On the other hand, when the concentration of the dyes (RB and R6G) increases from 0.008% to 0.1%, the respective broad excitation bands observed for the dilute samples are split into two bands observed between 300-350 nm and 350-425 nm respectively. In the excitation bands whose maxima lie between 300 and 350 nm, the peak position of the excitation spectrum of the sample doped with R6G is lower than the one doped with RB. However, the reverse situation is observed for the band between 350 nm and 425 nm. This splitting of the band is entirely due to the increase in concentration of the dye which increases the dye-dye and dye- di-ureasil interactions since the distances between them decrease [5].

Chapter 7: Conclusions

Fluorescent dyes were known for numerous applications in the area of optics, displays, biology, medicine, etc. For applications such as lasers and displays, it is important to incorporate the dye molecules in a suitable matrix which increases their optical performances and ease the portability of devices. There are number of matrices which could be used, but the organic inorganic hybrid materials are ideal materials which provide the dye molecules with matrix properties from organic and inorganic solid materials in one. The sol-gel synthesis route also makes the incorporation process of the dye molecule easy without affecting its original properties much.

In this work the doping of rhodamine dyes into an organic-inorganic hybrid materials classed as di-ureasil was done with the sol-gel synthesis route. The absorption, photoluminescence and X-ray diffraction characterization of the rhodamine 6G and B doped di-ureasil hybrid material were successfully performed. Both the di-ureasil and the dyes are optically active materials. As a result of this, the emission spectra of the samples doped with either of the dyes show double emission bands in the lower and higher wavelength regions. The one shown in the lower wavelength is the characteristic emission feature of the di-ureasil hybrid while the one shown in the higher wavelength region corresponds to the dye emission.

When the concentration of the dye increases the emission band from the di-ureasil was suppressed. This is due to an energy transfer from the di-ureasil emitting centers (urea bridge (NH) and siliceous domains) to the dye molecules. The presence of an energy transfer was also confirmed from the excitation spectra acquired by monitoring the emission wavelength from the emission band of the dye. Moreover, the severe suppression of the blue-green emission band of the di-ureasil emission shows that the energy transfer from the organic emitting centers is higher than the one from the inorganic emitting centers. This suggests the presence of large number of the dye molecules near the organic regions of the di-ureasil as compared to the siliceous domains.

The increase in the distance between the siliceous clusters for the doped di-ureasil, confirmed by XRD pattern, indicates the incorporation of the rhodamine molecules in the organic region of the di-ureasil.

Another effect of the increase in concentration of the dye is the shift in peak positions of the excitation, emission as well as absorbance spectra of the dyes compared to the peak positions observed for dilute concentration. These shifting in the peak positions of the dye for these optical techniques are showing the formation of different types of aggregates. The formation of aggregates was also seen with the dilute concentrations from the shoulders in the emission bands of dye. The Gaussian fitting performed on the spectrum further indicates the presence of the dimers which are the emitting centers for the shoulders.
The preserved emission profiles of the dye emission band in time resolved emission spectra show that the life time of the dye emission is comparable to the life time of the organic emitting centers of the di-ureasil. However, the accurate life time behind the emission can only be obtained by monitoring a decay curve around the observed band.
With respect to intensity, the emission of concentrated sample is very intense as compared to the dilute counterpart. This is related to the increase in emission intensity of the material with the increase in concentration of the emitting centers. The absolute emission quantum yield measurement also confirms that the increase in dye concentration increases the measured value of the quantum yields. Emission quantum yields, 65% for RB and 70% for R6G doped materials (both 0.1% concentration) show that the material doped with either of the dyes has reasonably high quantum yield which can qualify them as a promising candidate for light emitting application.
In general, the incorporation of the rhodamine dyes into the di-ureasil hybrid material is confirmed with the respective optical and structural characterization techniques. As the di-ureasil is an organic-inorganic hybrid material with the important properties of organic and inorganic components in one host for the organic dye, the material prepared here is of high importance for optical applications such as laser dyes. This is because the dye molecules entrapped into the organic region of the solid matrix have their optical properties more or less preserved. Furthermore, the energy transfer between the di-ureasil and the rhodamine dyes enables to change the broad emission spectra of the di-ureasil into a relatively narrow emission band located in the higher emission wavelength regions for both rhodamines.

References

[1]. a) S. E. San, O. Köysal, M. Okutan, *The Arabian Journal For Science and Engineering*, **30**, 337, 2005.

[2] H. Iwanaga, K. Naito, F. Effenberger, *Liquid Crystals*, **27**, 115, 2000.

[3]. S. Schultheiss, E. Yariv, R. Reisfeld and H. D. Breuer, *Photochem. Photobiol. Sci.,* **1**, 320, 2002.

[4]. http://finechem.dlut.edu.cn/05icfm/article/review/Development%20of%20Rhodamine%20Dyes%20for%20Biochemical.pdf, (retrieved, 05/06/09).

[5]. A. Kurian, N. A. George, B. Paul, V. P. N. Nampoori and C. P. G. Vallabhan, *Laser Chemistry* **20**, 99*,* 2002.

[6]. F. Rong-Wei , L. Xiao-Hui, X. Yuan-Qin, J. Yu-Gang, H. Wei-Ming, C. De-Ying, *Chin.Phys.Lett*., **25**, 1881, 2008.

[7]. K. Kuriki, T. Kobayashi, N. Imai, T. Tamura, Y. Koike, and Y. Okamoto, *Polym. Adv. Technol*.**11**, 621 (2000)

[8]. R. Reisfeld, A. Weiss, T. Saraidarov, E. Yariv and A. A. Ishchenko, *Polym. Adv. Technol.* **15,** 291, 2004

[9]. A. V. Deshpande, and E. B. Namdas, *Appl. Phys*. **B 64**, 419, 1997.

[10]. A. Mortensen, Concise Encyclopedia of Composite Materials, 2nd ed., Elsevier Ltd. Amsterdam, 2007.

[11] A. Costela, I. García-Moreno, D. del Agua, O. García, and R. Sastre, *Optics Journal* **1**, 1, 2007.

[12] .a) V. M. Martinez, F. L. Arbeloa, J. B. Prieto, and I. L. Arbeloa, *J. Phys. Chem. B* **109**, 7443, 2005.

b) V. M. Martinez, F. L. Arbeloa, J. B. Prieto, T. A. Lopez, and I. L. Arbeloa*, J. Phys. Chem. B* , 1**08**, 20030, 2004.

[13]. R. Saster and A. Costela, *Adv. Mater*. **7**, 190, 1995.

[14]. M. Canva, P. Georges, J.-F. Perlgritz, A. Brun, F. Chaput, and J. -P.Boilot, *Journal de physique IV*, **4**, 369, 1994

[15]. L. Hu and Z. Jiang, *Optics communications* **148**, 275, 1998.

[16].a) G. Kickelbick, Hybrid *Materials: Synthesis, Characterization, and Applications*, WILEY-VCH Verlag GmbH & Co. KGaA, Weinheim, 2007. b) P. Gomez-Romero, C. Sanchez, *Functional Hybrid Materials*; WILEY-VCH Verlag GmbH & Co. KGaA, Weinheim, 2004.

[17] . C. Sanchez, B. Julian, P. Belleville, and M.Popall, *J. Mater. Chem*., **15,** 3559, 2005.

[18] http://www.dstuns.iitm.ac.in/teaching-and- presentations/teaching/undergraduate%20courses/vy305-molecular-architecture-and-evolution-of-functions/presentations/presentations-2007/seminar-1/P4.pdf, (retrieved, 05/06/09).

[19] a) P. G. Romero, *Adv. Mater*. **13**, 163, 2001. b) http://en.wikipedia.org/wiki/Adobe (retrieved, 05/06/09). c) A. K. C. Gallegos, 'Organic inorganic hybrid materials based on conducting organic polymer as electrodes for energy storage devices' a PhD thesis *submitted* to: Laboratorio de Quimica del Estado Solido Instituto de Ciencie de Materiales, Oct. 2003, Barcelona.

[20] P. Judeinstein and C. Sanchez, *J. Mater. Chem*., **6**, 511, 1996,

[21] K. G. Sharp, *Adv. Mater*. **10,** 1243, 1998.

[22] M. H.V. Werts, *Luminescence Science Progress* **88**, 101, 2005.

[23] C. Sanchez, *J. Mater. Chem*., **15**, 3557, 2005.

[24] L. D. Carlos, R. A. S. Ferreira, V. de Zea Bermudez, and S. J. L. Ribeiro, *Adv. Mater.,* **20**, 1, 2008.

[25]. C. J. Brinker and G.W.Sherer, *Sol-gel science: the physics and chemistry of Sol-gel processing*, Academic press, San Diego CA, 1990.

[26]. L. D. Carlos, V. de Zea Bermudez, R. A. S. Ferreira, L. Marques, and M. Assuncüao, *Chem. Mater.* **11,** 581, 1999.

[27]. (a) http://www.psrc.usm.edu/mauritz/solgel.html, (b) http://en.wikipedia.org/wiki/Sol-gel, (c) http://optoweb.fis.uniroma2.it/opto/solgel/ (retrieved, 05/06/09).

[28] . Lianshe Fu, R. A. S Ferreira, N. J. O. Silva, L. D. Carlos, V. de Zea Bermudez, and J. *Rocha, Chem. Mater.* **16 (8),** 1507, 2004.

[29]. S. C. Nunes, V. de Zea Bermudez, J. Cybinska, R. A. S. Ferreira, L. D. Carlos, M. M. Silva, M. J. Smith, D. Ostrovskii, J. Rocha , *J. Mater. Chem.,* **15***,* 3876, 2005. [30]. V. de Zea Bermudez, L. D. Carlos, and L. Alccer*, Chem. Mater.* **11,** 569, 1999.

[31]. R. A. S. Ferreira, L.D. Carlos, V. de Zea Bermudez, *Thin Solid Film* **313-344,** 476, 1999.

[32]. L. D. Carlos, R. A.S. Ferreira, V. De Zea Bermudez, and S. J. L. Ribeiro, *Adv. Funct. Mater.*, **11**, 111, 2001.

[33]. G. Cao, Nanostructures *& nanomaterials; Synthesis, Properties and Application, Washington*, Imperial Collage Press, 2004.

[34] a) J. Mohan, *Organic spectroscopy: principles and applications*, 2nd ed., Norosa publishing house, New Delhi, 2001. b) P.L.Kriz, *Introduction to spectroscopy, 2nd ed*, Harcourt collage publishers Orlando FL, 2001. c) http://teaching.shu.ac.uk/hwb/chemistry/tutorials/molspec/uvvisab1.htm (retrieved, 05/06/09)

[35]. a) P. W. Atkins and R.S. Friedman, *Molecular quantum mechanics, 3rd ed.,* Oxford University Press; Oxford, NY, 1997. b) H. H. Telle, A. G. Urena And R. J. Donovan*, Laser chemistry: spectroscopy dynamic and application*, John Wiley and sons Ltd. England, 2007.

[36] B. Valeur, *Molecular Fluorescence: Principles and Applications*, Wiley-VCH Verlag GmbH, 2001.

[37] http://www.physik.unibas.ch/Praktikum/VPII/Fluoreszenz/Fluoresc ence_and_Phosphorescence.pdf, (retrieved, 05/06/09).

[38] D. C. Oliveira, A. G. Macedo, N. J. O. Silva, C. Molina, R. A. S. Ferreira, P. S. André, K. Dahmouche, V. De Zea Bermudez, Y. Messaddeq, S. J. L. Ribeiro, and L. D. Carlos, *Chem. Mater. **20**, 3696*, 2008.

[39] S. S. Nobre, P. P. Lima, L. Mafra, R.A. S. Ferreira, R. O. Freire, Lianshe Fu, U. Pischel, V. de Zea Bermudez, O. L. Malta, and L. D. Carlos, *J. Phys. Chem. C,* **111***,* 3275, 2007.

[40] K. Dahmouche, C. V. Santilli, S. H. Pulcinelli, and A. F. Craievich, *J. Phys. Chem. B* **103***,* 4937, 1999.

[41] A. S. Jaaskelainane and T. Liitia, *spectroscopy Europe*, **19**, 11 2007.

[42] Kasha, M., Rawls H. R., El-Bayoumi, M. A., *Pure Appl. Chem.* **11**, 371, 1965.

[43] F. Del Monte and D. Levy, *J. Phys. Chem.* B **103**, 8080, 1999.

[44] F. del Monte, J. D.Mackenzie, and D. Levy, *Langmuir*, **16**, 7377, 2000.

[45] F. del Monte, M. L. Ferrer, and D. Levy, *Langmuir*, **17**, 4812, 2001.

[46] C. M. Carbonaro, F. Meinardi, P. C. Ricci, M. Salis, and A. Anedda, J. *Phys. Chem.* **B**, **113**, 5111, 2009.

[47] L. D. Carlos, R. A. S. Ferreira, R. N. Pereira, M. Assuncüao, and V. de Zea Bermudez, *J. Phys. Chem. B* **108***,* 14924, 2004.

[48] R. A. S Ferreira, L. D. Carlos, R. R. Gonalves, S. J. L. Ribeiro, and V. de Zea Bermudez, *Chem. Mater.* **13***,* 2991, 2001**.**

[49] http://bcp.phys.strath.ac.uk/ultrafast/Blue_book/Red_Dyes.pdf, (retrieved, 05/06/09).

[50]] R.Vogel, P. Meredith, M.D. Harvey, H. R. Dunlop , *spectrochimica Acta part A* **60,** *245, (*2004).

[51] M. C. Gutierriz , M. J. Hortiguela, M. L. Ferrer, and F. del Monte *Langmuir,* **23**, 2175, 2007.

[52] T.Fujii H. Niromasa and T.Tamura, *Chem. Phys. Lett*. **233**, 424, 1995.

[53] M. L. Gomez, D. P. Fasce, R. J. J. Williams, H. A. Montejano, C. M. Previtali, *Journal of Polymer Science: Part B:* Polymer Physics, **46***,* 289, 2008.

[54] M. Sharma, D. Mohan, R.D. Singh, N. Singh, Optical *Materials* **30,** 1273, 2008

[55] R.A. S. Ferreira , L. D. Carlos, V. De Zea Bermudez, C. Molina, K. Dahmouche, Y. Messaddeq, and S.J.L. Ribeiro, J*ournal of Sol-Gel Science and Technology* **26**, 315, 2003

[56] M. C. Gonualves, V. de Zea Bermudez, R. A. S. Ferreira, L. D. Carlos, D. Ostrovskii, and J. Rocha, *Chem. Mater.* ***16****,* 2530, 2004.